

CZECH TECHNICAL UNIVERSITY IN PRAGUE
FACULTY OF MECHANICAL ENGINEERING
DEPARTMENT OF ENVIRONMENTAL ENGINEERING

AIR COOLING OF AN LED LIGHT SOURCE

MASTER'S THESIS

POLINA KIM

3-TPR-2024

I. OSOBNÍ A STUDIJNÍ ÚDAJE

Příjmení: **Kim** Jméno: **Polina** Osobní číslo: **508890**
Fakulta/ústav: **Fakulta strojní**
Zadávající katedra/ústav: **Ústav techniky prostředí**
Studijní program: **Technika prostředí**
Specializace: **Bez specializace**

II. ÚDAJE K DIPLOMOVÉ PRÁCI

Název diplomové práce:

Chlazení LED zdroje světla vzduchem

Název diplomové práce anglicky:

Air Cooling of an LED Light Source

Pokyny pro vypracování:

Vypracujte tepelně-technický návrh chladiče pro LED zdroj světla do zařízení pro optickou kontrolu elektronických desek. Pro parametrickou optimalizaci chladiče použijte nástroje simulačního softwaru ANSYS.

Seznam doporučené literatury:

Kraus A.D., Aziz A. and Welty J. Extended Surface Heat Transfer. New York : John Wiley & Sons, 2001.
Bar-Cohen A., Lyengar M., Kraus A. D. Design of Optimum Plate-Fin Natural Convective Heat Sinks. Transactions ASME, vol. 125, p.208-216, 2003. [DOI: 10.1115/1.1568361]
McCay O. et al. A Parametric Design Study of Natural-Convection-Cooled Heat Sinks. Fluids, vol. 8, no. 8, 2023. Dostupné z: <https://doi.org/10.3390/fluids8080234> [cit. 2022-03-12].
Ansys Fluent User's Guide. Canonsburg (PA) : ANSYS, Inc., 2023.
Ansys Fluent Theory Guide. Canonsburg (PA) : ANSYS, Inc., 2023.

Jméno a pracoviště vedoucí(ho) diplomové práce:

Ing. Martin Barták, Ph.D. ústav techniky prostředí FS

Jméno a pracoviště druhé(ho) vedoucí(ho) nebo konzultanta(ky) diplomové práce:

Datum zadání diplomové práce: **08.04.2024**

Termín odevzdání diplomové práce: **06.06.2024**

Platnost zadání diplomové práce: _____

Ing. Martin Barták, Ph.D.
podpis vedoucí(ho) práce

doc. Ing. Vladimír Zmrhal, Ph.D.
podpis vedoucí(ho) ústavu/katedry

doc. Ing. Miroslav Španiel, CSc.
podpis děkana(ky)

III. PŘEVZETÍ ZADÁNÍ

Diplomantka bere na vědomí, že je povinna vypracovat diplomovou práci samostatně, bez cizí pomoci, s výjimkou poskytnutých konzultací. Seznam použité literatury, jiných pramenů a jmen konzultantů je třeba uvést v diplomové práci.

Datum převzetí zadání

Podpis studentky

Summary

The master thesis is dedicated to the parametric optimization of a light source cooler. During the research, a literature review regarding heat sinks and various approaches to enhance their efficiency was carried out. A model of a heat sink with mounted LED strip was built using Ansys Design Modeler, and simulations of natural convection and thermal analyses were performed in the Ansys Fluent software. To validate the model, an experiment was conducted where the surface temperature of the existing heat sink was measured. Parametric optimization was carried out using the Ansys Direct Optimization tool. The optimized parameters were the fin height and the distance between them, with the objective of reducing the cooler's average surface temperature. As a result of the optimization, the cooler's surface temperature was reduced by 7.4 %. New methods for manufacturing the part were proposed, taking into account the values of the optimized parameters.

Souhrn

Diplomová práce se zabývá parametrickou optimalizací chladiče světelného zdroje. Během výzkumu byla provedena rešerše odborné literatury týkající se chladičů a různých přístupů k zlepšení jejich účinnosti. Model chladiče s LED páskem byl vytvořen v programu Ansys Design Modeler a simulace přirozené konvekce a tepelné analýzy byly provedeny v softwaru Ansys Fluent. K ověření modelu byl proveden experiment, při kterém byla měřena teplota povrchu existujícího chladiče. Parametrická optimalizace byla provedena pomocí nástroje Ansys Direct Optimization. Optimalizovanými parametry byla výška žebek a vzdálenost mezi nimi, s cílem snížit průměrnou povrchovou teplotu chladiče. V důsledku optimalizace došlo ke snížení teploty povrchu chladiče o 7,4 %. Byly navrženy nové metody výroby dílu s ohledem na hodnoty optimalizovaných parametrů.

Declaration

I declare that the diploma thesis entitled "Air Cooling of an LED Light Source" is my own work performed under the supervision of Ing. Martin Barták, Ph.D., with the use of the literature presented at the end of my diploma thesis in the list of references.

In Prague 05. 06. 2024

.....

Polina Kim

Acknowledgments

I would like to express appreciation to my thesis supervisor Ing. Martin Barták, Ph.D. for his persistent guidance and expert feedback. Thanks should also go to my colleagues and classmates for their valuable pieces of advice and help. Lastly, I am grateful to my family and friends for their care and moral support.

Table of Contents

Nomenclature	1
1. Introduction.....	2
2. LED thermal management	4
2.1. LED function and operation	4
2.2. Heat sink working principle	5
3. Optimization approaches.....	8
3.1. Existing optimization solutions for passive cooling.....	10
4. Natural convection heat transfer solution based on dimensionless correlations...	12
5. Natural convection heat transfer solution by CFD simulations	16
6. Optimization methods in Ansys.....	18
7. Problem description	22
8. Solution based on dimensionless correlations	25
9. Solution based on simulation	27
9.1. Model setup	27
9.1.1. Geometry	27
9.1.2. Meshing	28
9.1.3. Solver.....	30
9.2. Model validation.....	33
9.3. Optimization and parametric set.....	35
10. Results and discussions.....	37
10.1. Model validation.....	37
10.2. Optimization results.....	40
11. Conclusion	43
References	45
Appendix I. Thermal paste datasheet	47
Appendix II. PT100 thermometer tolerances	48
Appendix III. Ansys Direct Optimization setup.....	50

Nomenclature

A_s	$[m^2]$	heat sink surface area in contact with fluid
a	$[m^2 \cdot s^{-1}]$	thermal diffusivity
g	$[m \cdot s^{-2}]$	gravitational acceleration
h	$[W \cdot m^{-2} \cdot K^{-1}]$	average heat transfer coefficient
I	$[A]$	average current through an LED strip
L	$[m]$	fin height
L_c	$[m]$	characteristic length
n_d	$[-]$	number of diodes on an LED strip segment
P_{nom}	$[W]$	nominal power of an LED strip
\dot{Q}_{conv}	$[W]$	rate of heat transfer by convection
q_V	$[W \cdot m^{-3}]$	volumetric heat source of an LED strip
s	$[m]$	distance between two adjacent fins
T_e	$[K]$	temperature of the fluid outside a boundary layer
T_{HS}	$[K]$	average temperature of the heat sink surface
$T_{LED MAX}$	$[K]$	maximum temperature of an LED strip
T_m	$[K]$	average fluid temperature
T_s	$[K]$	average temperature of the surface
U	$[V]$	voltage of an LED
V	$[m^3]$	LED strip volume
Gr	$[-]$	Grashof number
Nu	$[-]$	Nusselt number
Pr	$[-]$	Prandtl number
β	$[K^{-1}]$	thermal expansion coefficient
λ	$[W \cdot m^{-1} \cdot K^{-1}]$	thermal conductivity
ν	$[m^2 \cdot s^{-1}]$	kinematic viscosity

1. Introduction

In recent decades, there has been a continuous trend towards decreasing electrical components' sizes, while their power is on the contrary increasing. According to Moore's law, every two years the number of transistors in an integrated circuit doubles. At the same time, the heat flux and the heat dissipation requirements are increasing reaching $500 \text{ W}\cdot\text{cm}^{-2}$ in 2024 [1].

For the operation of any electronic component, certain operating conditions are required. If these conditions are violated, the part will not function correctly or will fail altogether. According to [2] it is the violation of the correct temperature regime that is the most frequent cause of electronic element failures. With an increase in power, the heat generation of components also increases, and if the cooling parameters of the cooler are not improved, the electronics will overheat, which will invariably lead to failure.

Even though modern cooling systems are able to transfer heat loads as powerful as $10 \text{ MW}\cdot\text{m}^{-2}$ [3], many researchers are trying to investigate and introduce even more efficient heat transfer methods to improve the service life and device efficiency. While using new materials could lead to a larger safe temperature limit for electronic chips, this approach is currently over-priced. The industry is looking for other ways of increasing the overall heat transfer coefficient. Cooling methods are generally classified into active and passive techniques. While active cooling solutions rely on an external source, passive solutions benefit from free convection, radiation, no energy consumption and surface modifications to improve heat transfer.

The subject of this work is the cooler of a light source consisting of high-power light-emitting diodes (LED) soldered on a printed board circuit (PCB). The system is then implemented into the assembly line at the end of a certain stage of automated production to monitor the quality of the production and, if necessary, sort out or mark defective parts. Thus, the module is a subject of increased reliability requirements under continuous operation conditions since any breakdown or malfunction in serial production leads to the stoppage of the entire conveyor belt and massive loss of money. That is why proper thermal management of an LED strip is a critically important design task for the entire inspection system.

Design optimization of a cooler was made in the Ansys software which allows a user to solve a variety of complex problems in different physics fields. All steps needed for optimization from geometry creation to parametric study were made on the Ansys Workbench platform with utilization of such tools as Ansys Design Modeler, Ansys Meshing, Ansys Fluent and Direct Optimization.

The conducted research described in the thesis was made in cooperation with Wickon Hightech s.r.o. The company specializes in automated optical inspection (AOI) solutions for industrial applications. This introduced some manufacturing limitations to the problem as well as an opportunity to carry out experiments on the actual operating machine.

2. LED thermal management

2.1. LED function and operation

Light-emitting diode (LED) is a semiconductor device that converts electrical current into light emission. For better understanding of the heat emission caused by LED operation, a basic knowledge of its physics is necessary.

LED function is based on p-n junction phenomenon (see Figure 2.1). Through a process called doping, the n-type material becomes enriched with negative charge carriers (electrons), while the p-type material becomes enriched with positive charge carriers (holes). Two materials are in a close contact with each other creating a depletion zone that allows the current to flow only in one direction. A potential barrier V_0 , called the built-in voltage, prevents electrons from diffusing from the n-side to the p-side. When an electric field is applied to the diode, electrons and holes in the p- and n-type materials move towards the p-n junction. As excess electrons move from the n-type material to the p-type material and recombine with holes, energy E_g is released in the form of photons – elementary particles (quanta) of electromagnetic radiation. All diodes emit photons, but not all of them emit visible light. The material for an LED is chosen so that the wavelength of the emitted photons falls within the visible spectrum and corresponds to a certain light color.

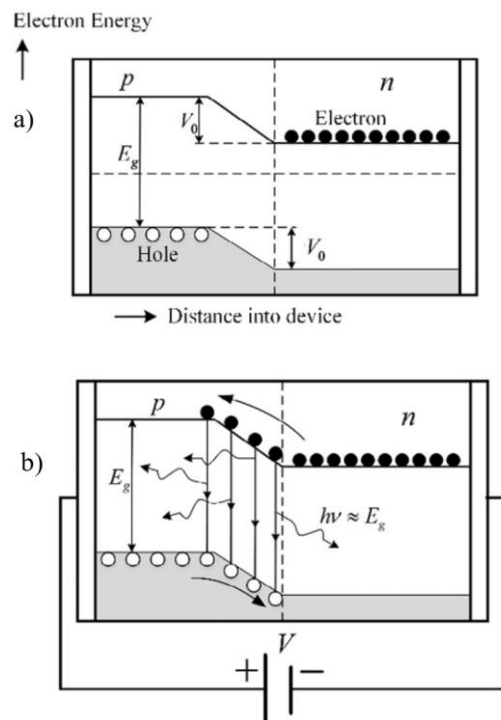


Figure 2.1. p-n junction principle before (a) and after (b) voltage application [4].

The beam of visible light emitted by an LED is considered "cold," but due to losses within LED, heat is generated at the p-n junction, sometimes to a significant extent. Two LED temperatures should be distinguished: the temperature on the crystal surface and in the p-n junction area. The surface temperature affects the lifespan of the device, while the p-n junction temperature impacts the light output. Generally, as the p-n junction temperature increases, the LED brightness decreases by up to 1 % per K [5] because the internal quantum efficiency drops due to crystal structure vibrations. The aging effect can lead to a further degradation as demonstrated in [6, 7].

Therefore, limiting the temperature of the p-n junction through properly designed heat dissipation and other temperature control methods is critical to ensure the normal operation of the LED, optimize its light output, and increase its lifespan.

2.2. Heat sink working principle

Heat sink is a vital component used in electronic devices to dissipate heat generated by electronic components such as processors, graphics cards, and power transistors. It typically consists of a metal or alloy base with fins of different shapes. When electronic components operate, they produce heat due to electrical resistance. A heat sink transfers this heat away from the component by conduction and then to the ambient environment by convection and radiation, allowing an electronic device to operate within safe temperature limits and prevent thermal damage.

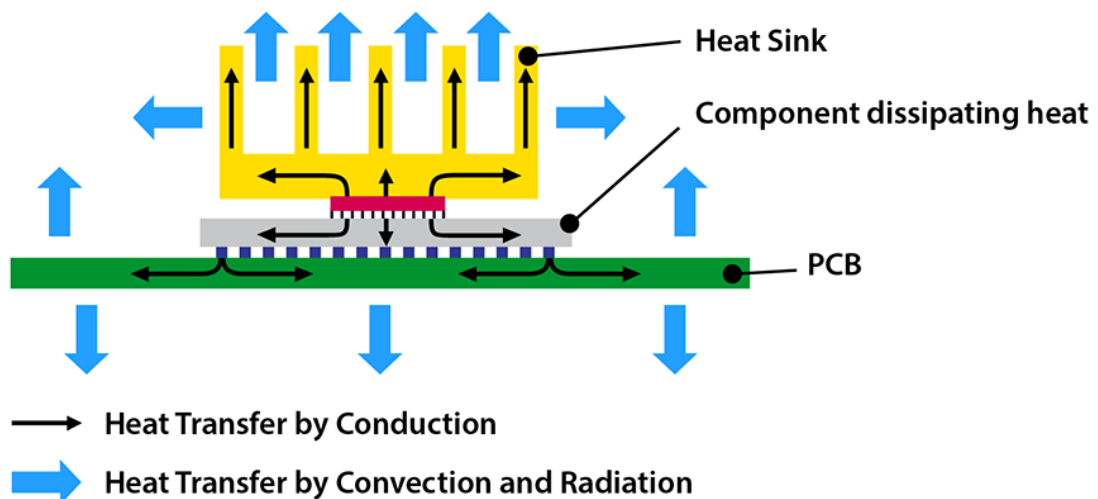


Figure 2.2. Heat flow in a typical heat sink [8]

Several key factors define performance of heat sinks:

- material;
- heat sink design;
- mounting technique;
- fluid environment;
- fluid flow around a heat sink;
- implementation of heat pipes and vapor chambers.

Choosing materials with higher thermal conductivity can significantly improve heat sink performance. These materials effectively conduct heat away from the electronic component to the rest of a heat sink. The most common materials for heat sink production are aluminum and copper since they are known for their high thermal conductivity ($200 \text{ W}\cdot\text{m}^{-2}\cdot\text{K}^{-1}$ and $385 \text{ W}\cdot\text{m}^{-2}\cdot\text{K}^{-1}$, respectively).

A larger surface area increases the heat exchange between a heat sink and surrounding fluid (air or coolant). This can be reached by adding more fins or other extended surfaces to the heat sink base, by optimizing fin design (length, thickness) or even by chemical roughening of the whole heat sink [16]. Additionally, fin density and placement influences airflow between fins and, subsequently, convective heat transfer.

Proper attachment of a cooled component to the heat sink is vital for efficient heat transfer. Two solid surfaces would come into contact not over the entire area, but only at some points. In such a case, heat transfer is much less efficient than if the space between the surfaces was filled with thermally conductive material. Various methods, including thermal interface materials (TIMs) or screws, ensure good thermal contact between the heat sink and the electronic component. TIMs, like paste or pads, are used to fill microscopic gaps between the heat sink and the electronic component, decreasing contact resistance and enhancing heat transfer efficiency.

The surrounding fluid can be either air or liquid (water, silicone oil, etc.). Air is the most used coolant as it is easily available, and the necessary equipment is simple and inexpensive. Liquid cooling is employed in high-performance computing and industrial applications where air cooling is insufficient. Liquids have higher thermal conductivity and specific heat capacity than air, leading to more intensive heat transfer.

Passive or active methods can be applied when using heat sinks. Passive cooling uses natural convection which occurs as a result of the density difference between a hotter fluid close to a heat sink and a cooler fluid in the surrounding environment. Although passive methods are reliable, simple and cheap, they are suitable for low-power applications only, reaching maximum heat transfer coefficient of $1 \text{ kW}\cdot\text{m}^{-2}\cdot\text{K}^{-1}$. For better cooling performance active method can be selected. This method incorporates fans or liquid cooling systems to further enhance heat dissipation. Heat transfer coefficient then reaches up to $40 \text{ kW}\cdot\text{m}^{-2}\cdot\text{K}^{-1}$ [8].

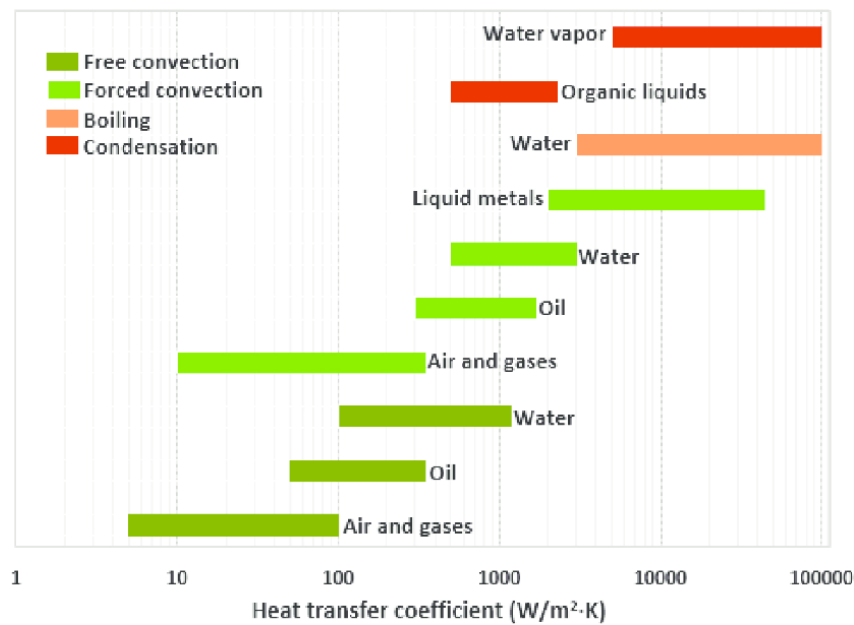


Figure 2.3. Heat transfer coefficient variation of different cooling methods

Integrating heat pipes or vapor chambers into the heat sink design can help to distribute heat more evenly across the heat sink surface. These technologies effectively transport heat away from the source to areas with higher airflow, improving overall heat dissipation. These systems increase heat flow or utilize phase-change cooling to remove heat more efficiently, especially in high-power applications.

3. Optimization approaches

Optimizing heat sink design involves maximizing the heat dissipation while minimizing the size, weight and cost. There are two main approaches to this problem: parametric and topological optimization. In the first case, the shape of the part is predefined. Parameters that describe the part are introduced, taking values within a specific range. Parametric optimization involves altering these parameters to find the extremum of an objective function dependent on them, within given constraints. The optimal parameters are those at this extremum. In topological optimization, the mathematical algorithm determines the shape of the future part by gradually removing material from the initial "full" domain. It maximizes or minimizes the target parameters while ensuring the fulfilment of the system of constraints. As a result, the shape of the part has a unique form with complex structures, such as internal channels, ribs and others. Such geometry is often impossible to manufacture using traditional methods. However, modern technologies, such as 3D printing, allow topological optimization to be considered an effective way to improve parts. A combination of the two optimization methods is sometimes used. In the initial stage of redesign, the part undergoes topological optimization. Then, based on the resulting shape, a form that can be manufactured using traditional machines is determined. Finally, parametric optimization of the new geometry is performed.

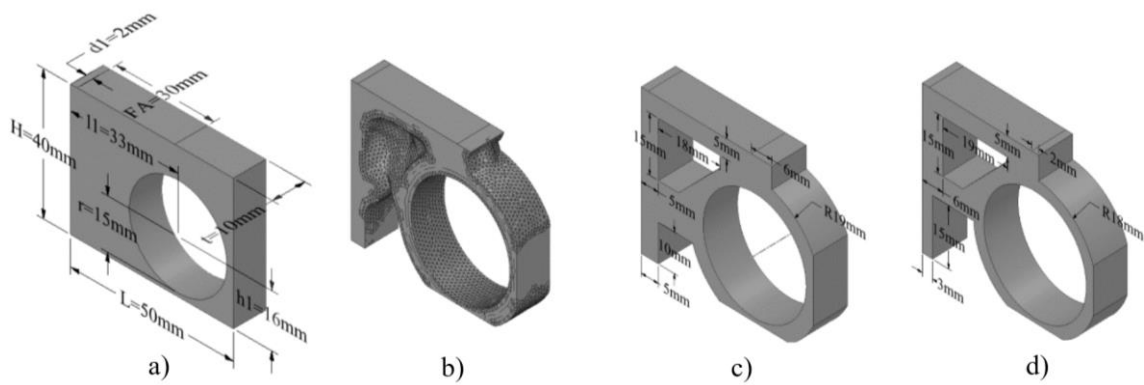


Figure 3.1. An evolution of a part design: a – initial design, b – after topological optimization, c – redesign with manufacturability considerations, d – after parametric optimization [25]

From a mathematical perspective, there are three methods for solving optimization problem:

1. optimization algorithms,
2. iterative methods,
3. heuristics.

Iterative methods belong to exact methods, which means that an optimal solution achievement is guaranteed when using such an approach. A common example of an iterative algorithm is the gradient-based optimization. This method is used to find the minimum or maximum of a function by iteratively moving in the direction defined by the gradient of an objective function. Gradient-based methods are particularly effective for problems where the objective function is smooth and differentiable [9]. Even though iterative methods succeed in finding the exact solution, they require massive computational resources. Heuristic methods, in contrast to the previous approaches, do not necessarily find an exact optimal solution but reduce running time drastically when dealing with more complex problems [10]. This approach is applied, for instance, in genetic algorithms. These algorithms are inspired by the process of natural selection and evolution. A population of designs represented as “genomes” is generated. After that it undergoes mutation, crossover, and selection processes to iteratively improve performance with respect to a given quality measure. Genetic algorithms can efficiently explore large design spaces and find near-optimal solutions to complex optimization problems.

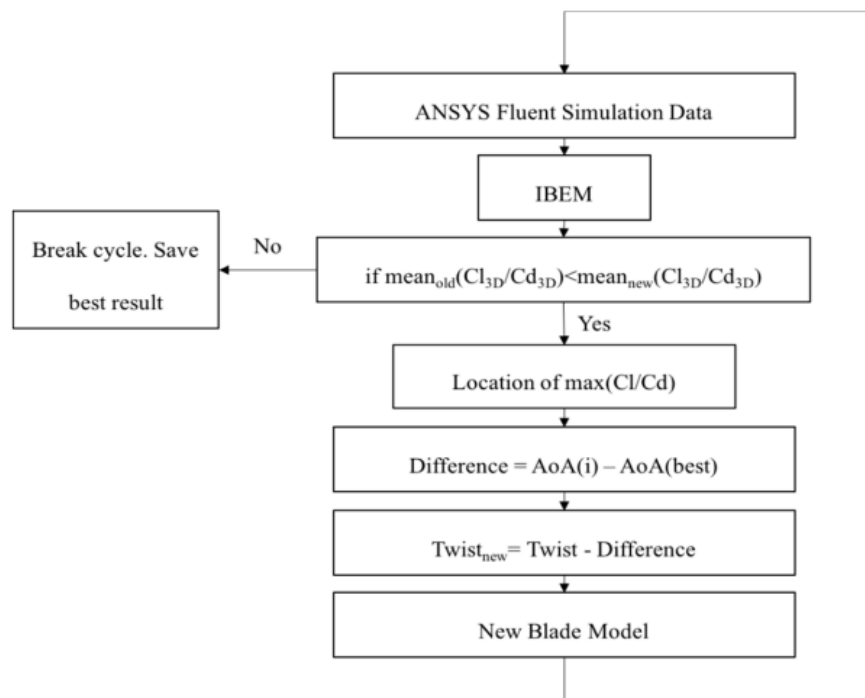


Figure 3.2. An example of the algorithm for wind turbine blade design optimization [11]

Computational methods are powerful tools for design optimization. However, experimental prototyping and testing remain essential for validating improvements as

physical testing allows to verify simulation results, identify potential discrepancies, and improve designs for real applications.

3.1. Existing optimization solutions for passive cooling

Numerous scientific studies have been dedicated to exploring various ways of improving heat sink performance.

Costa and Lopes [12], for example, were working on a geometry improvement of the heat sink for an LED lamp under natural convection by numerical simulations. They reached a core temperature reduction of 22.65 °C keeping it under required limit of 65 °C by optimizing fins' height, length and number.

Culham and Muzychka [13] introduced an optimization model based on the minimization of entropy generation allowing one to adjust geometric parameters of a heat sink, material and heat dissipation properties as well as flow conditions within one optimization process. Forced convection could be incorporated into the procedure in addition. The described method effectiveness was then demonstrated on several examples where the convergence was reached under certain constraints.

Dede et al. [14] in their studies presented topology optimization of an air-cooled heat sink. The optimization objective was to minimize thermal compliance function which represents thermal potential energy. The main difficulty of such approach is manufacturing complexity of the final design. In the second part of the research a production of such a shape using additive layer manufacturing technology was presented. A similar study was made by Pilagatti et al. [15] showing the efficiency of this method and verifying the manufacturability of such geometry by using laser-powder bed fusion technology.

Ghazi et al. [16] conducted an experimental study of roughening the surface of an aluminum heat sink with heat pipes under passive cooling conditions. The results of atomic force microscopy analysis showed that the average roughness of chemically treated fins was 59 ± 3 nm, which is significantly larger than that of the initial surface (7.6 ± 5 nm). Heat sink etching led to the increase of surface area and, as a result, to the maximum temperature reduction of 7.2 °C.

Habib et al. [17] analyzed the influence of fin geometry and structure on heat transfer rate under natural convection. They introduced the macro channel 'L-shaped heat

sink'. An experimental and numerical study revealed a decrease of the average thermal resistance by 12 % when using an L-shaped composition of fins.

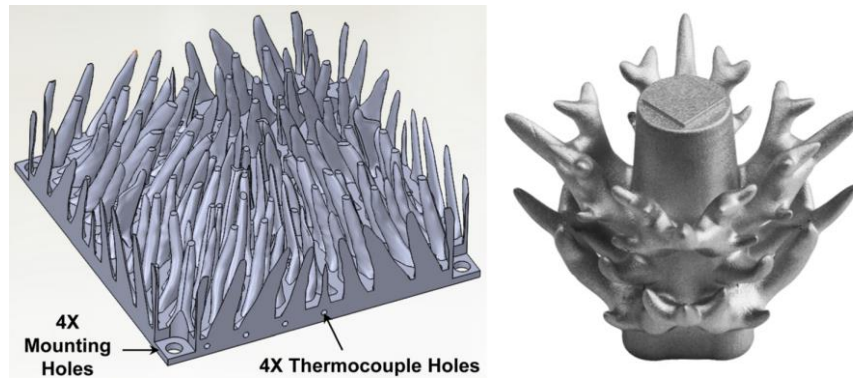


Figure 3.3. Shapes generated by topology optimization methods [14, 15]

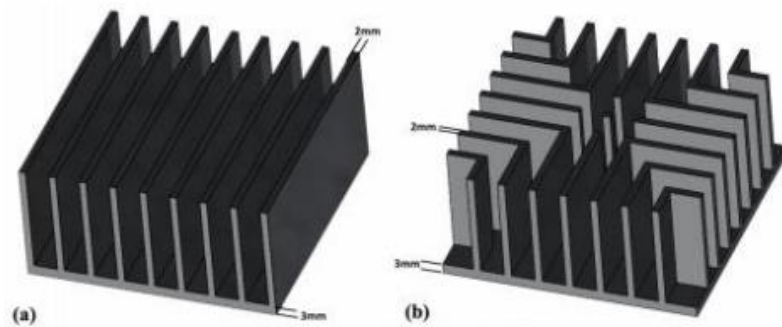


Figure 3.4. A conventional fin heat sink (a) and L-shaped fin heat sink (b) [17]

4. Natural convection heat transfer solution based on dimensionless correlations

The amount of heat removed by a cooler is determined mostly by the rate of heat transfer through convection from the cooler's surface to the surrounding fluid, that can be calculated using the following formula:

$$\dot{Q}_{conv} = h \cdot A_s \cdot (T_s - T_e) \text{ [W]} \quad (1)$$

where h [$\text{W} \cdot \text{m}^{-2} \cdot \text{K}^{-1}$] is the average heat transfer coefficient, A_s [m^2] is the heat transfer surface area in contact with fluid, T_s [K] is the average temperature of the surface and T_e [K] is the temperature of the fluid outside a boundary layer.

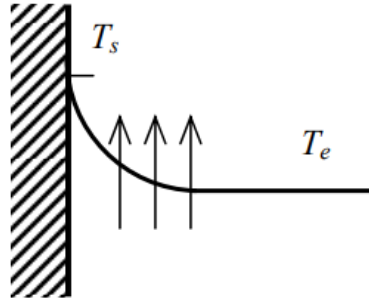


Figure 4.1. Temperature field in a fluid flowing along a wall of a higher temperature [18]

Since the heat transfer coefficient depends on several factors, its value is determined either experimentally or from empirically derived dimensionless correlations. The Nusselt number (Nu) correlation includes a heat transfer coefficient. It is a function of Grashof (Gr) and Prandtl (Pr) numbers in case of natural convection. The definitions of these numbers are as follows:

$$Nu = \frac{h \cdot L_c}{\lambda} = f(Gr, Pr) \text{ [-]} \quad (2)$$

$$Gr = \frac{g \cdot \beta \cdot (T_s - T_e) \cdot L_c^3}{\nu^2} \text{ [-]} \quad (3)$$

$$Pr = \frac{\nu}{a} \text{ [-]} \quad (4)$$

where h [$\text{W} \cdot \text{m}^{-2} \cdot \text{K}^{-1}$] is the average heat transfer coefficient,

L_c [m] is the characteristic length depending on a surface geometry,

λ [$\text{W} \cdot \text{m}^{-1} \cdot \text{K}^{-1}$] is the fluid thermal conductivity,

g [$\text{m} \cdot \text{s}^{-2}$] is the gravitational acceleration,

$\beta [K^{-1}]$ is the thermal expansion coefficient,
 $T_s [K]$ is the average temperature of the surface,
 $T_e [K]$ is the temperature of the fluid outside a boundary layer,
 $\nu [m^2 \cdot s^{-1}]$ is the kinematic viscosity,
 $a [m^2 \cdot s^{-1}]$ is the thermal diffusivity.

In natural convection problem solutions, the Nusselt number can be also correlated to the Rayleigh number (Ra), which is a product of Gr and Pr :

$$Nu = C \cdot Ra^n \quad (5)$$

$$Ra = Gr \cdot Pr = \frac{g \cdot \beta \cdot (T_s - T_e) \cdot L_C^3}{\nu \cdot a} [-] \quad (6)$$

where $C [-]$ and $n [-]$ are parameters dependent on the geometry of the surface and the flow regime.

A great number of experimental studies were dedicated to these dimensionless correlations for a variety of geometry and flow configurations. The most basic geometries are vertical and horizontal plates. When the Nusselt number over a vertical plate is calculated, its height is taken as the characteristic length. In case of a horizontal plate, the characteristic length is the ratio of the surface area A_s over its perimeter p . Another common configuration that could be useful for heat sink calculations is a narrow channel between two vertical plates (a spacing between plates s is much smaller than their length L in the flow direction) – see Figure 4.2. If the longitudinal size of plates L is small (or the channel width s is large), the boundary layers might not merge in the middle of the channel and the problem can be solved as for two separate vertical plates. Otherwise, those layers will affect each other and should be analyzed concurrently. The average Nusselt number semi-empirical correlations for natural convection over surfaces of these geometries [19]:

- Vertical plate (Figure 6 a):

$$Nu = 0.59 \cdot Ra^{\frac{1}{4}}, Ra = 10^4 \text{ to } 10^9 \quad (7)$$

$$Nu = 0.1 \cdot Ra^{\frac{1}{3}}, Ra = 10^{10} \text{ to } 10^{13} \quad (8)$$

$$Nu = \left(0.825 + \frac{0.387 \cdot Ra^{\frac{1}{6}}}{\left(1 + (0.492/Pr)^{\frac{9}{16}} \right)^{\frac{8}{27}}} \right)^2, \text{ the entire range of } Ra \quad (9)$$

- Horizontal plate (upper surface of a hot plate or lower surface of a cold plate) (Figure 6 b):

$$Nu = 0.59 \cdot Ra^{\frac{1}{4}}, Ra = 10^4 \text{ to } 10^9 \quad (10)$$

$$Nu = 0.1 \cdot Ra^{\frac{1}{3}}, Ra = 10^{10} \text{ to } 10^{13} \quad (11)$$

- Horizontal plate (lower surface of a hot plate or upper surface of a cold plate) (Figure 6 c):

$$Nu = 0.27 \cdot Ra^{\frac{1}{4}}, Ra = 10^5 \text{ to } 10^{11} \quad (12)$$

- Gap between two vertical parallel plates (Figure 6 d):

$$Nu = \left(\frac{576}{\left(Ra_s \cdot \frac{S}{L} \right)^2} + \frac{2.873}{\left(Ra_s \cdot \frac{S}{L} \right)^{0.5}} \right)^{-0.5} \quad (13)$$

where

$$Ra_s = \frac{g\beta(T_s - T_e)s^3}{\nu^2} Pr \quad (14)$$

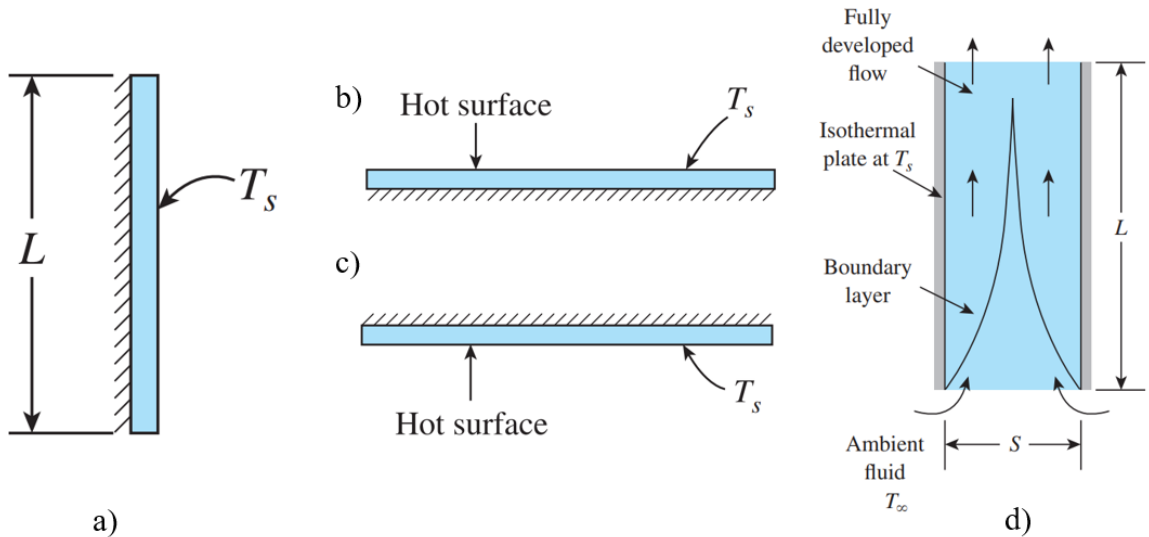


Figure 4.2. Geometry representations. Vertical plate (a), horizontal plates where hot surface is on top (b) and on bottom (c) side of a plate, two parallel plates (d) [19]

Defining the optimal distance between two adjacent fins on a heat sink (or two vertical plates in a simplified problem) is a common task in the heat sink optimization process. Placing more fins with smaller spacing on a given base area will increase the surface area A_s , but lower the heat transfer coefficient h in equation (1) as smaller gaps between two plates hinder the development of air flow in the channels. On the contrary, larger distance between fins will reduce their amount, leading to surface area decrease, while the air flow will go through the heat sink easier, causing an increase of the heat transfer coefficient. Thus, there is an optimum spacing s_{opt} that provides the maximum heat transfer from a heat sink with given base area [20]:

$$s_{opt} = 2.714 \cdot \left(\frac{s^3 \cdot L}{Ra_s} \right)^{0.25} = 2.714 \cdot \frac{L}{Ra_L^{0.25}} \text{ [m]} \quad (15)$$

$$Ra_L = \frac{g\beta(T_s - T_e)L^3}{\nu^2} Pr = Ra_s \frac{L^3}{s^3} \text{ [-]} \quad (16)$$

where s [m] is the distance between two adjacent fins,

L [m] is the fin height.

All the above correlations are valid under several assumptions:

- The fins are isothermal;
- The fin thickness t is small relative to the fin spacing s ;
- All fluid properties are evaluated at the average temperature $T_m = \frac{T_s + T_e}{2}$.

5. Natural convection heat transfer solution by CFD simulations

A sophisticated method of natural convection analysis is the computational fluid dynamics (CFD). CFD simulation can provide detailed insights into the temperature and velocity fields as well as turbulence and flow characteristics within the fluid and on the walls. Modern software, such as Ansys Fluent, allows a user to construct complex physical models choosing from a variety of settings making the solution as accurate as possible for a given problem. In a typical CFD simulation of natural convection, the following steps are usually involved:

1. Geometry and mesh are generated.

The physical domain is defined by creating a geometric model. The geometry is then discretized into a finite number of control volumes, forming a mesh. The quality of the mesh significantly affects the accuracy of the simulation. Finer meshes provide more detailed solutions but require more computational resources, so it is reasonable to predefine zones with higher accuracy requirements and refine mesh in those zones only.

Geometry and mesh generation are made in Ansys in a special software – Ansys Design Modeler or Ansys SpaceClaim for model creation and Ansys Meshing for mesh generation, where a huge variety of settings is presented from element size to meshing method. It offers automatic or manual meshing approaches allowing a user to generate optimal mesh for a specific task.

2. Governing equations of fluid dynamics are included into a calculation.

These equations are representing the three laws of conservation: conservation of mass (continuity equation), conservation of momentum (Navier-Stokes or Reynolds-Averaged Navier-Stokes equations) and conservation of energy (energy equation).

3. Appropriate boundary conditions are applied to the model.

For natural convection, typical boundary conditions include specified temperatures or heat fluxes on the walls, and possibly symmetry or periodic boundaries depending on the geometry. The no-slip condition is usually applied to solid boundaries, ensuring that the fluid velocity at the wall is zero.

4. Solution method is chosen.

The CFD solver uses numerical methods to solve the basic equations in either a coupled approach, when all equations are solved in one system within one iteration, or a segregated approach, when a problem solution is divided into subtasks that are solved sequentially. The choice of solver, such as pressure-based or density-based, depends on the nature of the flow and the specific problem. The former solver is used for incompressible flows at low speeds, whereas the later one – for high-speed compressible flows.

5. Turbulence model is selected.

Turbulence can play a significant role in natural convection. Ansys Fluent offers a variety of turbulence models that could be selected for a solution. The choice depends on flow specifics as well as available computational resources.

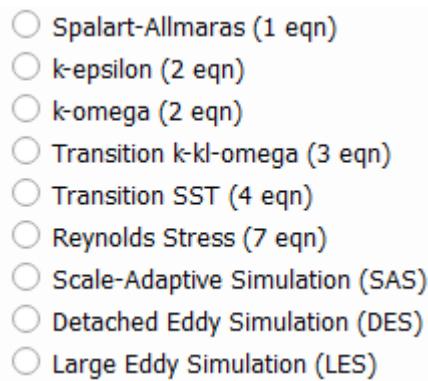
- 
- Spalart-Allmaras (1 eqn)
 - k-epsilon (2 eqn)
 - k-omega (2 eqn)
 - Transition k-k-omega (3 eqn)
 - Transition SST (4 eqn)
 - Reynolds Stress (7 eqn)
 - Scale-Adaptive Simulation (SAS)
 - Detached Eddy Simulation (DES)
 - Large Eddy Simulation (LES)

Figure 5.1. A list of turbulence models in Ansys Fluent

6. Simulations are performed.

The process goes iteratively, solving the equations for each time step or until a steady-state solution is achieved. Convergence criteria are defined to ensure that the solution is stable and accurate.

7. The simulation results are analyzed using post-processing tools.

The simulation results should be validated and interpreted using key parameters such as temperature distribution, velocity vectors, heat fluxes etc.

6. Optimization methods in Ansys

Ansys provides users with a wide range of sophisticated tools for both topological and parametric optimization. Direct method and response surface method can be employed for parametric optimization approach. The direct optimization method works with a certain number of experimental design points, solving them individually to achieve specific objectives. The optimal solution is reached iteratively by adjusting design parameters of a model. This approach is computationally intensive and has a low solution efficiency. Response surface optimization constructs explicit approximate expressions to replace implicit constraints or objective functions in the original design problem, significantly improving the optimization efficiency [21].

The optimization tools can be integrated into the Ansys Workbench Schematic. For a parametric optimization, a Parameter Set is created by selecting input or output parameters in single bundles. The range of optimized parameters' values, problem objectives and constraints are defined in the optimization block. Results and preliminary analytics are presented in that module as well.

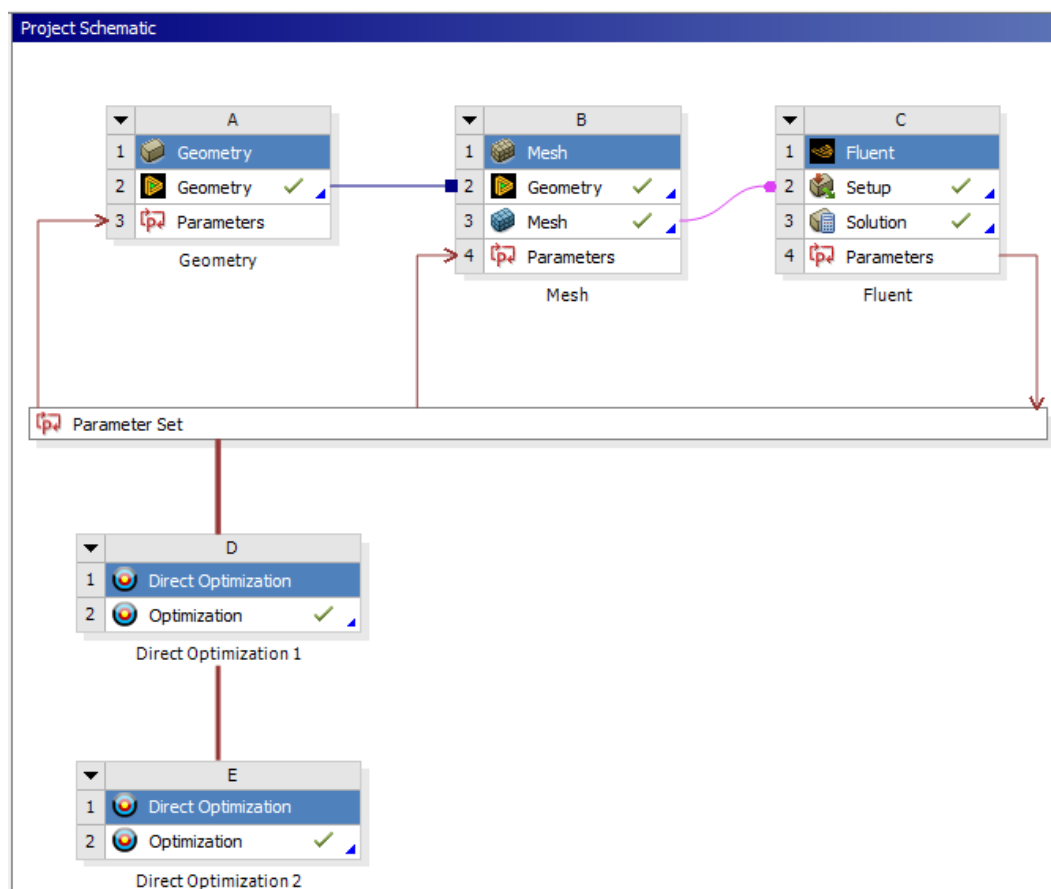


Figure 6.1. Example of Project Schematic with Parameter Set and Optimization blocks

Outline of Schematic F2: Optimization			
	A	B	C
1		Enabled	Monitoring
2	Optimization		
3	Objectives and Constraints		
4	Minimize P32		
5	P33 <= 363 K		
6	Domain		
7	HS v10 (A1)		
8	P34 - FinHeight	<input checked="" type="checkbox"/>	
9	P35 - FinSpace	<input checked="" type="checkbox"/>	
10	Parameter Relationships		
11	Raw Optimization Data		
12	Convergence Criteria		
13	Results		
14	Candidate Points		
15	Tradeoff		
16	Samples		

Figure 6.2. Example of an optimization outline

A variety of methods is offered within Ansys Workbench software for a parametric optimization process (descriptions are cited from the Ansys software documentation without modifications [22]):

- *The Screening optimization method* uses a simple approach based on sampling and sorting. It supports multiple objectives and constraints as well as all types of input parameters. Usually it is used for preliminary design, which may lead a user to apply other methods for more refined optimization results.
- *The MOGA method (Multi-Objective Genetic Algorithm)* is a variant of the popular NSGA-II (Non-dominated Sorted Genetic Algorithm-II) based on controlled elitism concepts. It supports multiple objectives and constraints and aims at finding the global optimum.
- *The MISQP method (Mixed-Integer Sequential Quadratic Programming)* solves mixed-integer nonlinear programming problems by a modified sequential quadratic programming (SQP) method. Under the assumption that integer variables have a smooth influence on the model functions, i.e. function values do not change drastically when in- or decrementing an integer variable, successive quadratic approximations are applied. It supports a single objective and multiple constraints. The starting point must be specified to determine the region of the design space to explore.
- *The Adaptive Multiple-Objective method* is a variant of the popular NSGA-II (Non-dominated Sorted Genetic Algorithm-II) based on controlled elitism

concepts. It supports multiple objectives and constraints and aims at finding the global optimum. It is limited to continuous and manufacturable input parameters.

- *The Adaptive Single-Objective method* is a gradient-based algorithm to provide a refined, global, optimization result. It supports a single objective, multiple constraints and aims at finding the global optimum. It is limited to continuous and manufacturable input parameters.

In the beginning of an optimization process, several cases (design points, DP) are determined. The initial number of design points and their configuration depend on the chosen optimization method. Each case has individual combination of chosen input parameters. Parameters from the table are automatically applied on the simulation model: geometry, meshing and solver bundles are updated and result columns (output parameters) are filled in. This optimization loop is repeated until all cases have an output value.

	A	B	C	D	E
1	Optimization	Enabled	Monitoring		
2	Objectives and Constraints				
3	Domain				
4	Geometry (A1)				
5	P34 - FinHeight	<input checked="" type="checkbox"/>			
6	P35 - FinSpace	<input checked="" type="checkbox"/>			
7	Parameter Relationships				
8	Raw Optimization Data				
9	Convergence Criteria				
10	Results				
11	Tradeoff				
12	Samples				

	A	B	C	D	E
1	Name	P34 - FinHeight (mm)	P35 - FinSpace (mm)	P32 - temperature-hs-op (K)	P33 - t_max_led-op (K)
2	1 DP 20	17	2,2	⚡	⚡
3	2 DP 21	13	2,6	⚡	⚡
4	3 DP 22	14	3,7	⚡	⚡
5	4 DP 23	18	4,1	⚡	⚡
6	5 DP 24	12	4,4	⚡	⚡
7	6 DP 25	19	2,9	⚡	⚡
8	7 DP 26	11	3,3	⚡	⚡
9	8 DP 27	16	4,8	⚡	⚡

Figure 6.3. Table of initial design points in the beginning of an optimization process (the lightning icons indicate that the output parameters are not updated yet)

Further design points may be added throughout an optimization process automatically. The total number of cases is determined by such optimization properties as number of initial samples, maximum number of evaluations, convergence criterion (only for non-genetic algorithms) and others. An automatic method selection is also possible in the Workbench tool. In that case a run time index regulates the number of samples. A larger number of evaluations bring higher possibility to find an optimal solution, yet it is more time consuming. Faster optimization solutions with a smaller design points variety may not assure reaching the best parameters' values, but may be useful for preliminary proposals.

Figure 6.4. Optimization properties of Adaptive Single-Objective method chosen manually (on the left) and automatically (on the right)

Figure 6.5. Optimization properties of MOGA method

After completion of the optimization process, candidate points are selected based on the degree to which the target parameters have been achieved. An additional candidate point may be entered manually and considered to be the optimal solution.

Table of Schematic E2: Optimization , Candidate Points								
	A	B	C	D	E	F	G	H
1	Reference	Name	P34 - FinHeight (mm)	P35 - FinSpace (mm)	P32 - temperature-hs-op (K)		P33 - t_max_led-op (K)	
2					Parameter Value	Variation from Reference	Parameter Value	Variation from Reference
3	☉	Starting Point <small>DP 13</small>	12	3	✗✗ 317,41	0,00 %	★★★ 318,03	0,00 %
4	☉	Candidate Point 1	20	3,1	✗✗ 314,9	-0,79 %	★★★ 315,82	-0,70 %
5	☉	Candidate Point 2	14	3	✗✗ 316,78	-0,20 %	★★★ 317,42	-0,19 %
6	☉	Candidate Point 3 <small>DP 13</small>	12	3	✗✗ 317,41	0,00 %	★★★ 318,03	0,00 %
*		New Custom Candidate Point	15	3,5				

Figure 6.6. Candidate Points table

7. Problem description

The main task of the thesis was to optimize an existing heat sink on which an LED strip is mounted. The PCB with diodes is connected to the cooler through thermal paste for better heat conduction. The technical parameters of the paste are specified in Appendix I.

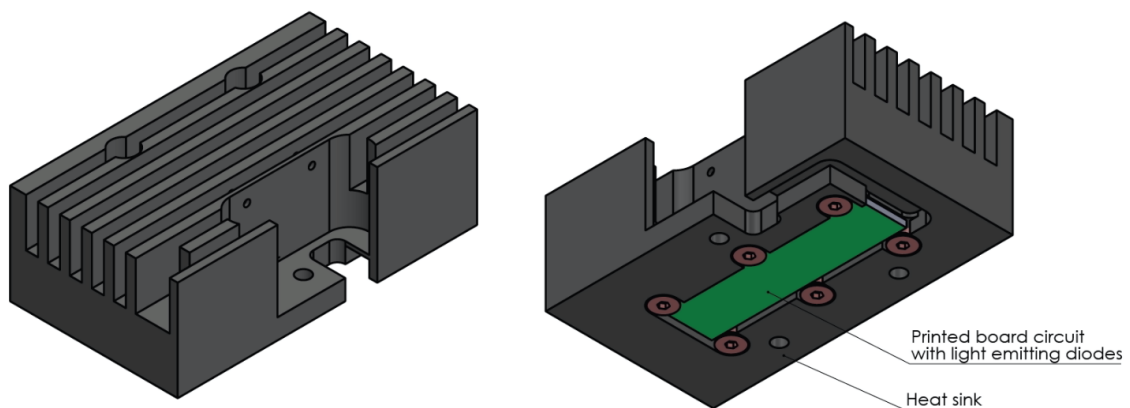


Figure 7.1. Illumination module assembly

The whole module is attached to the rest of the assembly with three screws. There are optical elements (lenses, prisms, apertures, etc.) inside the assembly which have to be placed in a correct position with tolerances of down to 0.02 mm. Temperature changes in the module lead to changes in the positions of these elements, and to incorrect operation of the device.

Thus, the task of the cooler is not only to remove heat in order to maintain the functionality of the LED strip itself, but also to limit deformations in the body of the object due to thermal changes.

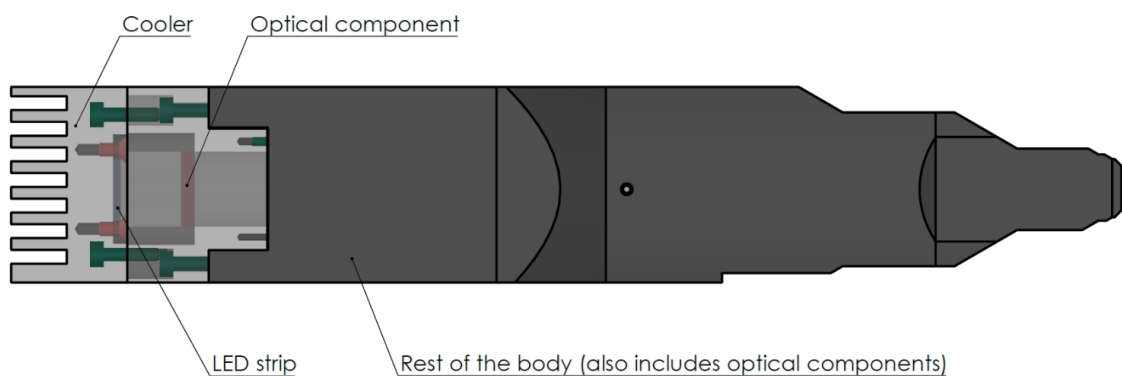


Figure 7.2. Complete light tool assembly

The light tool in Figure 7.2 is one of the components comprising the inspection head (sensor). In terms of heat exchange, the sensor contains not only the main light tool but also a camera and auxiliary lights mounted at the bottom of the head. Neither the camera nor the lights are continuously turned on. The camera captures images at specific intervals. The lights illuminate sequentially during the camera's exposure.

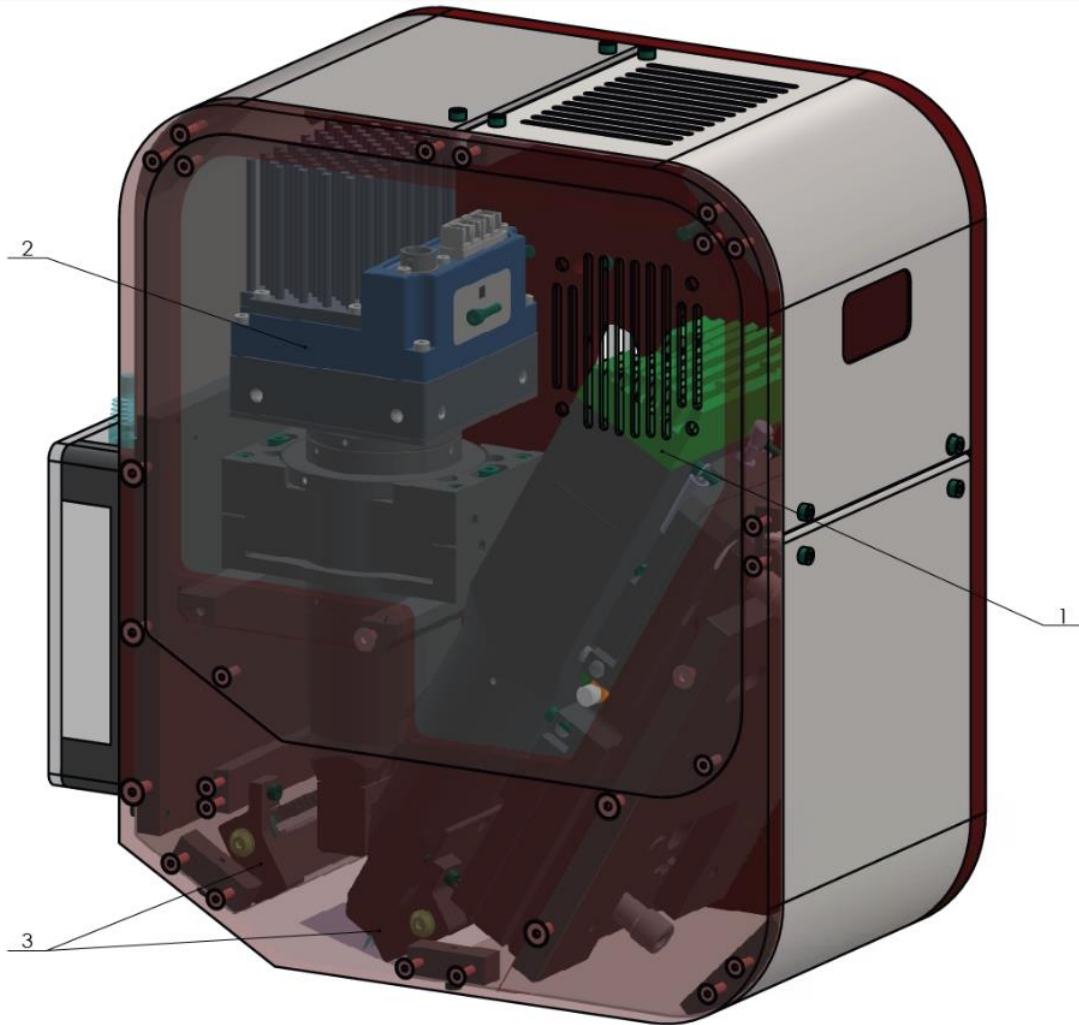


Figure 7.3. Inspection head assembly. Heat sources: main light (1), camera (2) and auxiliary lights (3). The optimized cooler is highlighted in green.

The machine uses passive cooling with aluminum heat sinks. The dimensions are determined by the overall dimensions of the assembly and available space as well as the capabilities of the manufacturer (width and depth of the milling tool, material). In passive cooling, most of the heat is removed by air flow driven by natural convection.

One way to improve the cooling capabilities of the heat sink is to change its material. Copper, for example, has almost two times higher thermal conductivity than aluminum ($385 \text{ W}\cdot\text{m}^{-2}\cdot\text{K}^{-1}$ and $200 \text{ W}\cdot\text{m}^{-2}\cdot\text{K}^{-1}$, respectively). By replacing the cooler with

a copper one, we would achieve better heat removal from the strip and the entire module. This option, however, was not considered due to manufacturing limitations. Wickon Hightech s.r.o. only mills aluminum parts in production, so designing a copper part would be impractical.

Another option to significantly increase the heat removal from the module would be to use *active cooling*. For example, a fan installed in front of the cooler would create air flow for more intense heat exchange between the cooler and the environment. However, this would significantly increase the requirements for electrical installation, making the entire module more expensive. Moreover, the main purpose of the machine is the automated optical inspection of microchips with a resolution of up to $2.5\ \mu\text{m}$. Strong air flow would contribute to unwanted circulation of dust particles in the space with inspected products. Even if the machine is installed in a clean room, the aluminum parts may undergo corrosion over time releasing microscopic particles, or small dust pieces may appear due to friction of moving parts.

Further way to improve cooler efficiency is to increase its surface area by increasing roughness using a chemical method. This solution, however, is too expensive considering the logistics and time spent on transportation and the additional step in creating the part.

Thus, it was decided to optimize the cooling capabilities of the cooler by changing its design. Two parameters were selected for optimization: fin spacing and fin height. The total height of the heat sink remains constant.

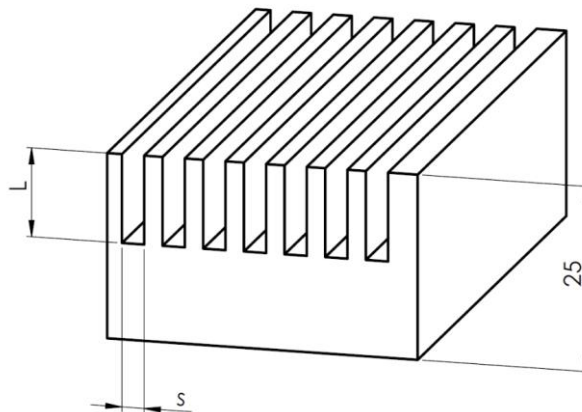


Figure 7.4. Cooler parameters for optimization – fin spacing s and fin height L

8. Solution based on dimensionless correlations

In this part of the thesis only one parameter was optimized – fin spacing. The calculations were made under the following assumptions:

- The temperature of the ambient air $T_e = 30 \text{ }^\circ\text{C}$;
- The fins were isothermal, the average fin surface temperature $T_s = 36.8 \text{ }^\circ\text{C}$ (obtained from the reference case simulation);
- All fluid properties were evaluated at the average temperature $T_m = \frac{T_s + T_e}{2} = 34.4 \text{ }^\circ\text{C}$;
- The atmospheric pressure was 100 kPa;
- Initial design had the following dimensions – see Figure 8.1.

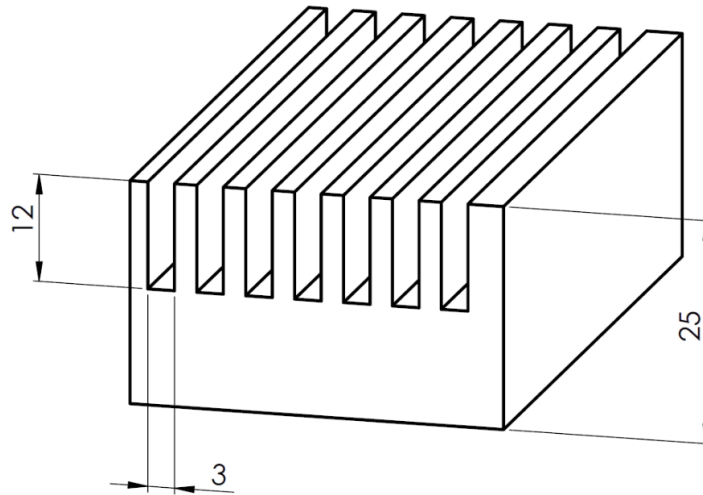


Figure 8.1. Initial cooler design parameters

Air properties at the temperature $34.4 \text{ }^\circ\text{C}$ and 100 kPa pressure:

$$\beta = \frac{1}{T_m [K]} = 0.00326 \text{ K}^{-1}$$

$$\nu = 1.64 \cdot 10^{-5} \text{ m}^2 \cdot \text{s}^{-1}$$

$$a = 2.29 \cdot 10^{-5} \text{ m}^2 \cdot \text{s}^{-1}$$

$$Pr = \frac{\nu}{a} = 0.713$$

Then the Rayleigh number for a fin height L as the characteristic length is, according to (16):

$$Ra_L = \frac{g\beta(T_s - T_e)L^3}{\nu^2} Pr = 1002$$

Low Rayleigh number means that the natural convection flow around the heat sink is weak in this case.

The optimum fin spacing was then calculated from (15):

$$s_{opt} = 2.714 \cdot \frac{L}{Ra_L^{0,25}} = 5.8 \text{ mm}$$

9. Solution based on simulation

The heat sink optimization was elaborated using the Ansys program, which provides sophisticated mathematical ground for calculating thermal processes and performing parametric optimization. The model with the original design was created and validated by experimental measurements. Following that, heat sink parameters optimization was performed. Geometry creation, meshing and optimization were set in the Ansys Workbench environment with Ansys Fluent as the solver. Ansys Direct Optimization tool was used for parametric optimization.

9.1. Model setup

9.1.1. Geometry

A model of the simulated system was built in Ansys Design Modeler software. The model consisted of a cooler, an LED strip and a part representing the rest of the assembly to which the cooler with the strip were screwed.

The ambient conditions were represented by air volume around the model. The domain was 15 mm wider than the heat sink on each side and 55 mm higher. The whole domain size was $72 \times 24 \times 150 \text{ mm}^3$. Modelling the entire inspection head, including other assemblies, air inlets and outlets, would result into more precise calculation outcome. However, this would also significantly increase computational requirements. A separate volume was added to simulate air in the cavity inside the part.

To reduce the mesh size and consequently the simulation time, the geometry of the objects was simplified. Thread holes and threads were not included in the model, as well as chamfers and recess fillets.

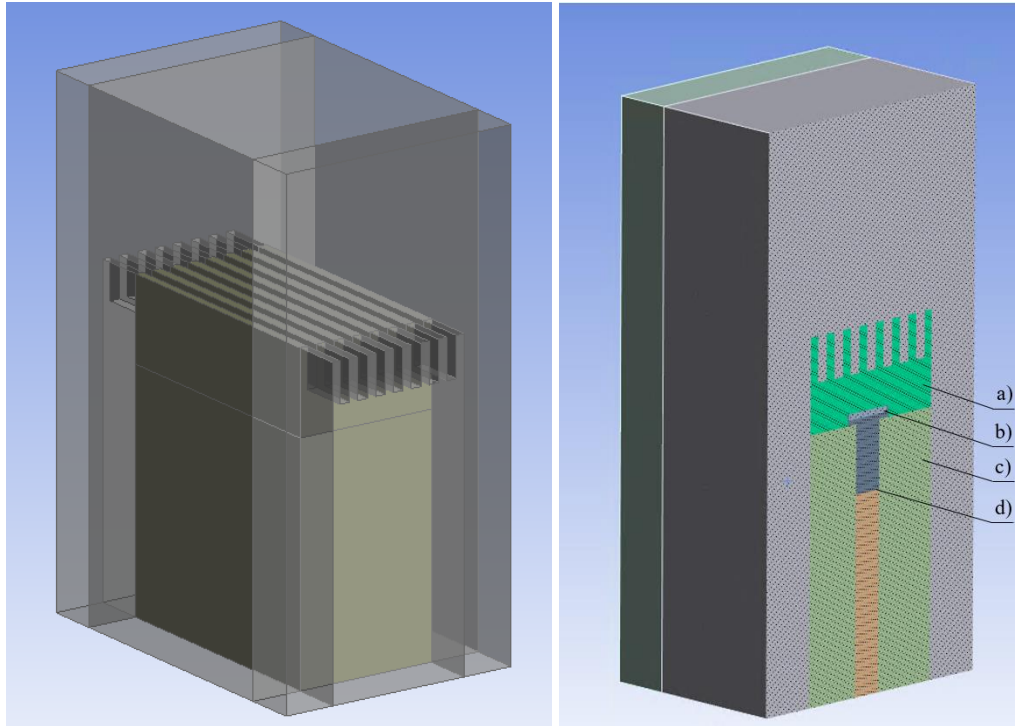


Figure 9.1. Built geometry (whole model and cut).
a – heat sink, b – LED strip, c – body, d – air cavity

9.1.2. Meshing

Computational mesh was generated in Ansys Meshing software.

The maximum element size was set to 1 mm. On certain surfaces the maximum element size was reduced to 0.15 mm. Therefore, there were at least 3 nodes through the thickness of each layer according to general rules for building a computational grid. Using Share Topology operation in the previous step made the generated mesh conformal. This means that in contact locations between two bodies the nodes of their elements were coincident, no "hanging nodes" were created. Such a grid allowed the solver to perform calculations accurately as well as reduced the calculation time.

The computational mesh for natural convection simulations has increased requirements for cells near to the cooled surface on the air side. At least the two first cells adjacent to the surface should be in the viscous sublayer. It means that y^+ in the closest cell to the surface should be around 1 [23]. To achieve this, an inflation operation was used in Ansys Meshing.

In this step individual surfaces were designated as named selections to indicate areas that behave differently from the heat transfer point of view (have different heat transfer coefficients). The following surfaces were assigned different settings: outer

surfaces (transverse and longitude), horizontal walls in channels, vertical walls in channels, upper surfaces of heat sink ribs.

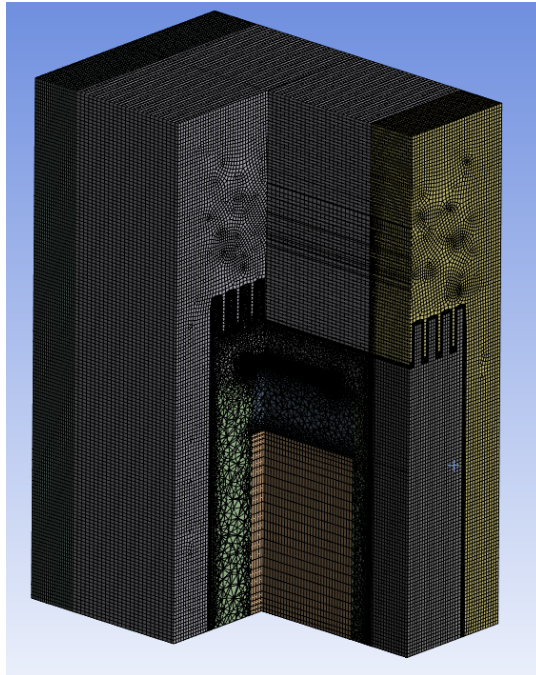
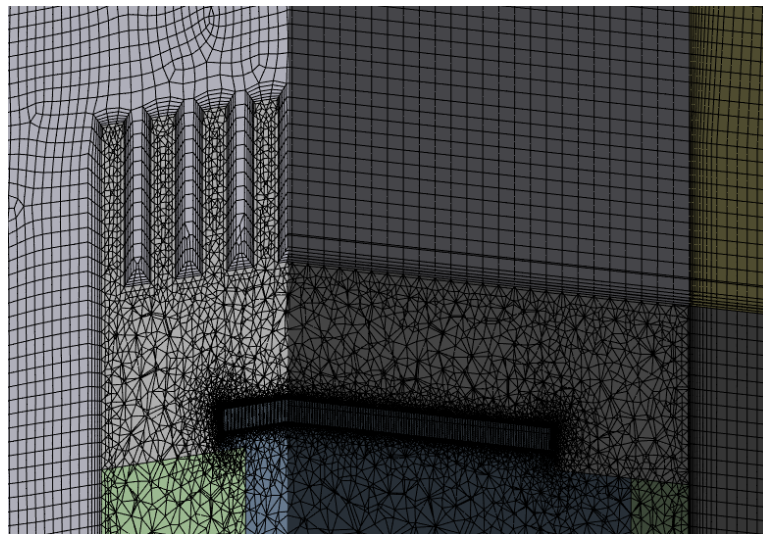


Figure 9.2. Generated mesh (whole model and cut)



*Figure 9.3. Generated mesh, double section view
(a closer look on areas with inflation and finer mesh)*

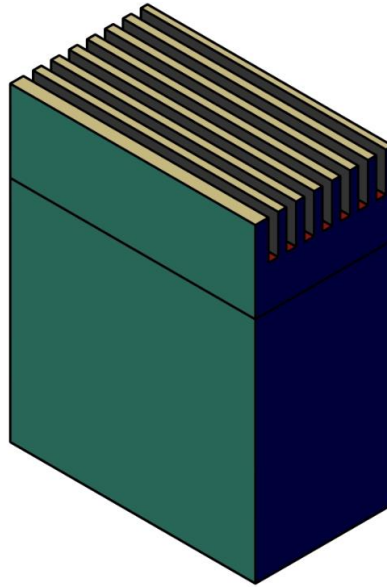


Figure 9.4. Named selections. Green – Wall_outer_long, blue – Wall_outer_short, yellow – Wall_upper, red – Channel_h, gray – Channel_v

9.1.3. Solver

The generated computational mesh was loaded into the solver – Ansys Fluent. A correct set up of the model had to be made in the solver – material properties, operational and boundary conditions, contact surfaces between bodies etc. A pressure-based coupled solver was used for simulations.

The operating temperature was set to 30 °C, operating pressure to 101325 Pa. Since the heat sink is tilted by 15 degrees from the vertical position, gravitational acceleration was divided into 2 components – along X and Z axis. The operating conditions are presented in the figure below.

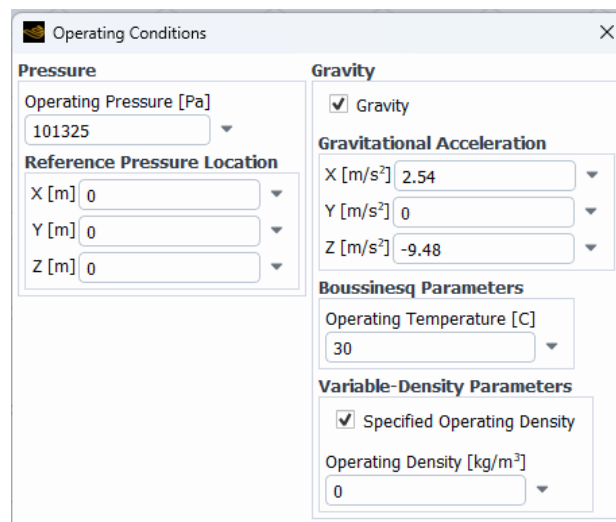


Figure 9.5. Operating conditions

The used materials were aluminum and air. To make natural convection simulation possible, air density was chosen to be a value dependent on temperature and independent on pressure (the flow is incompressible). Thermal conductivity and viscosity were set as polynomial functions of temperature for a more precise solution.

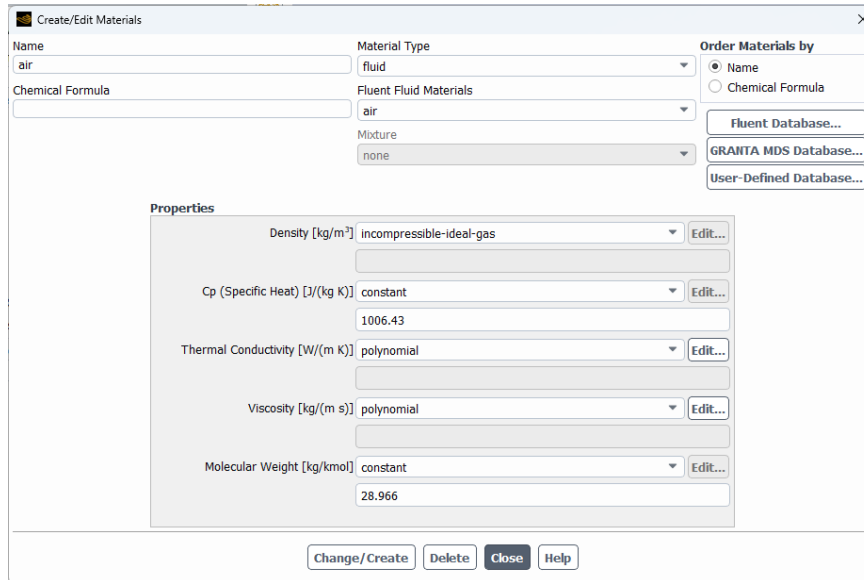


Figure 9.6. Air properties

The energy equation was included in the calculations to simulate thermal processes. Flow and turbulence equations were also activated for natural convection simulation. The k - ω GEKO [24] turbulence model was selected as the most suitable for this task.

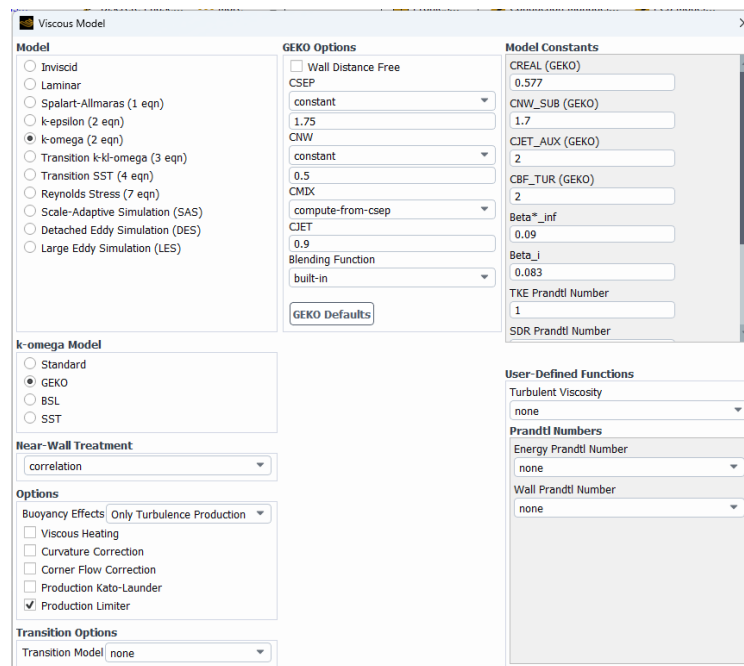


Figure 9.7. Viscous model setup

Heat transfer occurred by conduction (within bodies) and convection (on their surfaces). Two models of heat transfer by radiation presented in Ansys Fluent could be considered: the Surface-to-Surface (S2S) and the Discrete Ordinates (DO) radiation models. Since the S2S model can be applied on a model with constant surface mesh, and optimization process involves mesh regeneration for each case, this method is not suitable. The DO model, however, would be too computationally intensive. For these reasons, heat transfer by radiation was neglected in this problem.

The cooler is attached to the next component by three M3 screws, which create a pressure of 24 atm between the parts. The thermal contact resistance between them is then $0.4 \text{ m}^2 \cdot \text{K} \cdot \text{W}^{-1}$. No TIM is applied in this contact location since heat transfer from the cooler to the remaining assembly is undesirable. The Thermal Grizzly Hydronaut paste, 0.1 mm thick, is applied between the LED strip and the cooler. The technical specifications of the paste are provided in Appendix I. A material with thermal conductivity $11.8 \text{ W} \cdot \text{m}^{-1} \cdot \text{K}^{-1}$ was created and named “Thermal Paste”. Both contact zones (between the cooler and the component, between the strip and the cooler) were considered in the simulation.

The LED strip acts as a heat source in the study. It consists of 39 diodes. Each diode operates at the voltage of 2 V and an average current of 0.3 A. The maximum current is 0.7 A. Approximately 30 % of the electrical power is then converted to light and around 70 % to heat [4]. The diodes were turned on and off simultaneously and emitted light for about 4 % of the total duty cycle, which lasted 4 s. Thus, the volumetric heat source in the strip was $0.65 \text{ MW} \cdot \text{m}^{-3}$ according to the following equation.

$$q_v = \frac{I \cdot U \cdot n_d}{V} \cdot 0.7 \cdot 0.04 \left[\frac{\text{W}}{\text{m}^3} \right] \quad (17)$$

where I is the average current through an LED strip [A],

U is the voltage of an LED [V],

n_d is the number of diodes on an LED strip [-],

V is the LED strip volume [m^3].

9.2. Model validation

The CFD initial design model was validated in respect of accuracy. A temperature measurement experiment was conducted on the actual scanning machine (inspection head). The results were then compared to the simulated ones.

The scanning process was carried out as follows: a product with the length of 60 mm was moving on a vacuum table at the speed of $40 \text{ mm}\cdot\text{s}^{-1}$. At each $5 \text{ }\mu\text{m}$ shift of the product, the camera captured three images with the time interval of $1 \text{ }\mu\text{s}$. During the first frame, the main light operated for $10 \text{ }\mu\text{s}$, during the second frame, the main light ran for $5 \text{ }\mu\text{s}$, and during the third frame, auxiliary light sources illuminated the product. The time intervals of one frame cycle are depicted in Figure 9.8. After the product was scanned, the table moved back to the initial position and the whole process started again. The total duration of one scanning cycle was 4 s. The scanning took place in the first 1.25 s. During the remaining time, the table moved back to its starting position.

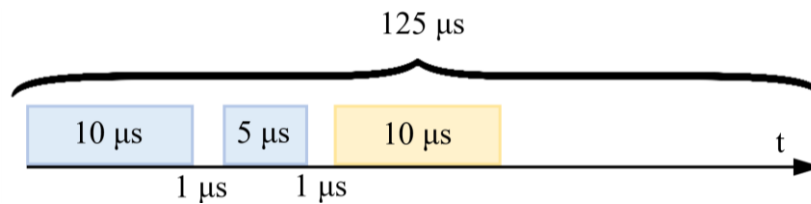


Figure 9.8. One shift cycle. Blue color is representing studied LED illuminating time, yellow color – additional lights illumination

The measurements were carried out using resistance temperature detectors (RTDs). RTDs' operation is based on the change in the resistance of precious metals due to temperature variations. Such metals exhibit a close to linear resistance characteristic. By supplying a constant current to the sensor, the change in resistance (and thus temperature) can be derived from the change in voltage. Four Pt-100 thermometers were soldered and assembled using Ahlborn ZA 9000-FS3 connectors, 4-wire cables and platinum sensors with the nominal resistance of $100 \text{ }\Omega$. The Pt100 thermometer tolerance at $40 \text{ }^\circ\text{C}$ is $\pm 0.5 \text{ }^\circ\text{C}$ in accuracy class B (see Appendix II). The soldered contacts were wrapped with insulating tape to prevent short circuits and inaccurate measurement results. Adapters on the opposite ends of the wires were connected to a portable data acquisition unit ALMEMO 2690. Two sensors were measuring air temperature (100 mm below the heat sink and 50 mm above it), two others were mounted on the heat sink surface with two-sided thermal tape (on the camera side and on the opposite one).

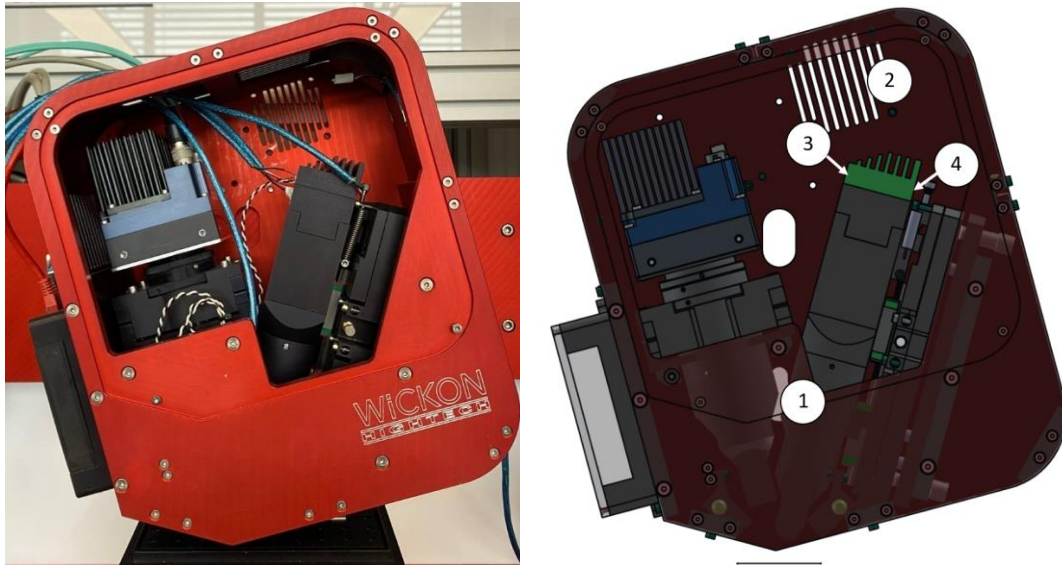


Figure 9.9. Experimental configuration. 1, 2 – air temperature sensors, 3, 4 – heat sink surface temperature sensors

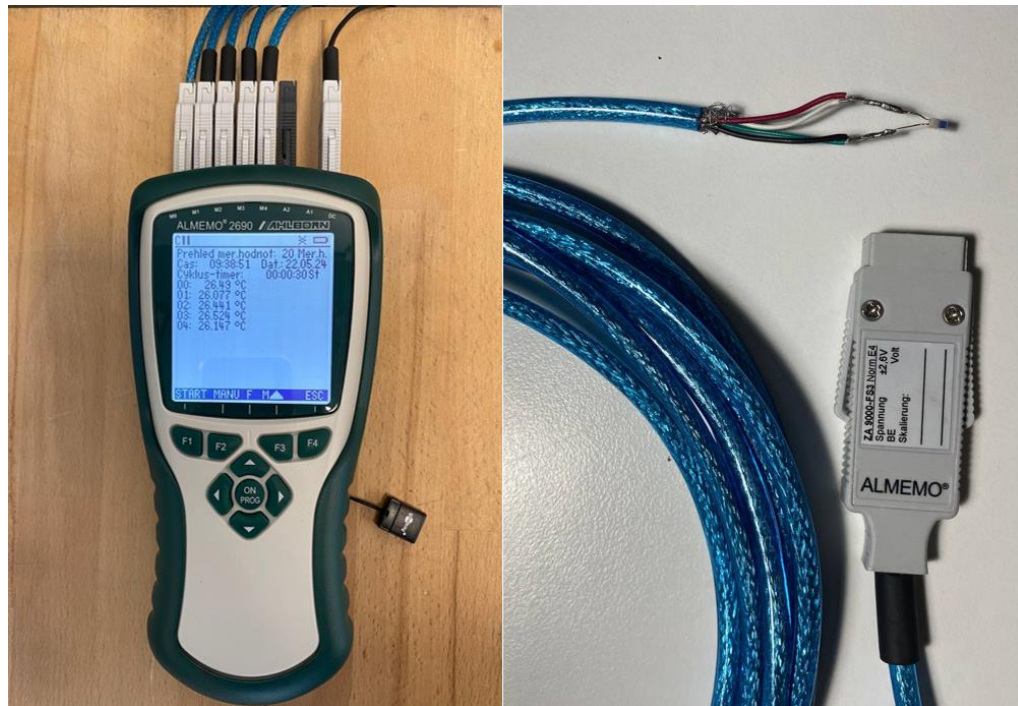
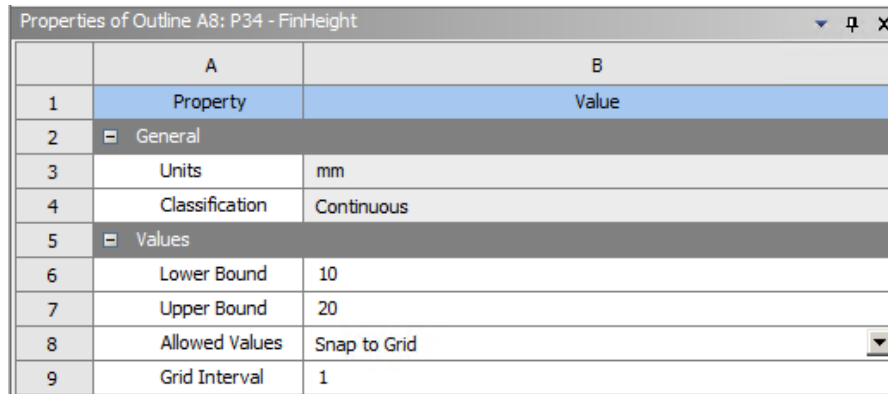


Figure 9.10. Measuring device ALMEMO 2690 (on the left) and a connector with soldered sensor Pt-100 (on the right)

Each connector was programmed in the software ALMEMO-Control to measure temperature within the range of -8 to $+60$ °C. Additionally, the ALMEMO measuring instrument was equipped with a memory card for recording data into a text file. Measurements were taken every 5 minutes to follow the temperature increase and read the necessary data when the temperature is stabilized. Measurement results are presented in Chapter 11.

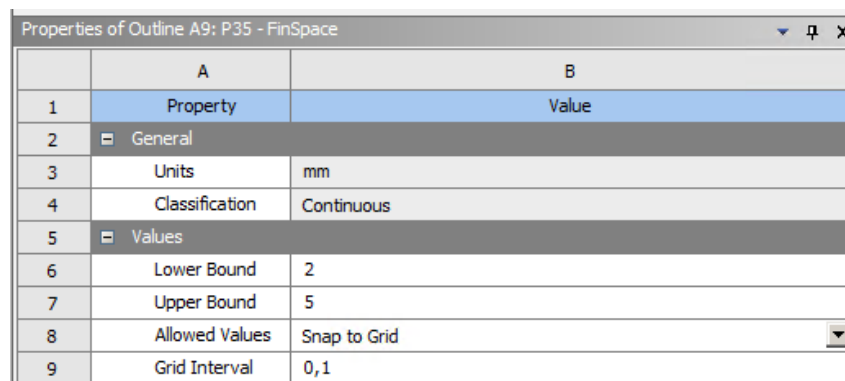
9.3. Optimization and parametric set

Two heat sink dimensions were selected as optimization parameters: the fin height L and the distance between the fins s . The height of the fins could vary from 10 to 20 mm and the fin space from 2 to 5 mm. These limits are determined by manufacturing constraints and assembly size requirements (available space in the complete system). Both parameters' allowed values were also limited by "Snap to grid" option with a grid interval 1 mm (height) and 0.1 mm (spacing).



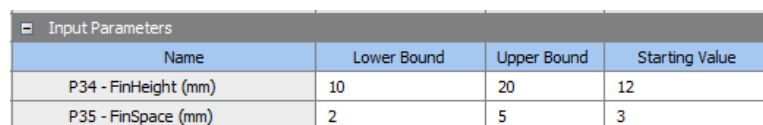
	A	B
1	Property	Value
2	General	
3	Units	mm
4	Classification	Continuous
5	Values	
6	Lower Bound	10
7	Upper Bound	20
8	Allowed Values	Snap to Grid
9	Grid Interval	1

Figure 9.11. Fin height parameter settings



	A	B
1	Property	Value
2	General	
3	Units	mm
4	Classification	Continuous
5	Values	
6	Lower Bound	2
7	Upper Bound	5
8	Allowed Values	Snap to Grid
9	Grid Interval	0,1

Figure 9.12. Fin spacing parameter settings



Input Parameters			
Name	Lower Bound	Upper Bound	Starting Value
P34 - FinHeight (mm)	10	20	12
P35 - FinSpace (mm)	2	5	3

Figure 9.13. Input parameters table

Optical elements, which are sensitive to displacement, are situated within the components attached to the cooler. It is critically important to limit the deformations of these components resulting from heat emitted by the LED strip during the operation process. A temperature change of up to 20 degrees is allowed for a proper device function. Moreover, it is necessary to ensure that the temperature of the LED does not

exceed the maximum operating value (100 °C). Thus, the optimization target parameters were the average temperature on the heat sink surface T_{HS} , and the maximum temperature of the LED strip $T_{LED MAX}$. The optimization task was to reduce T_{HS} while ensuring that $T_{LED MAX}$ does not exceed the value of 363 K (i.e. 90 % of the maximum value).

Table of Schematic F2: Optimization									
	A	B	C	D	E	F	G	H	I
1	Name	Parameter	Objective			Constraint			
2			Type	Target	Tolerance	Type	Lower Bound	Upper Bound	Tolerance
3	Minimize P32	P32 - temperature-hs-op	Minimize	0		No Constraint			
4	P33 <= 363 K	P33 - t_max_led-op	No Objective			Values <= Upper Bound		363	0,001
*		Select a Parameter							

Figure 9.14. Optimization objectives and constraints setup

The reference case revealed that the system is in a safe zone in terms of temperature, taking into account the current LED heat power. Therefore, it was decided to increase volumetric heat source of an LED strip from $0.65 \text{ MW}\cdot\text{m}^{-3}$ to $8 \text{ MW}\cdot\text{m}^{-3}$ as if it was active for 50 % of cycle time. This change raised the observed temperatures and their potential reduction. Input and output parameters of the initial (reference) case are presented in the table below:

Table 1. Initial case parameters

Parameter	h, mm	s, mm	T_{HS} , °C	$T_{LED MAX}$, °C
Value	12	3	44.3	44.9

Considering that there is only one constraint in the optimization problem, the Adaptive Single-Objective optimization model was chosen with the number of initial samples equal to 6.

10. Results and discussions

10.1. Model validation

Temperature development is shown in the Figure 10.1, the final stabilized temperatures are presented in the table below.

Table 2. Temperature values acquired experimentally

#	Channel number	Description	Steady temperature, °C
1	00	Air temperature 100 mm below the heat sink	29.3 ± 0.5
2	01	Air temperature 50 mm above the heat sink	30.9 ± 0.5
3	02	Temperature of the heat sink surface from the camera side	35.8 ± 0.5
4	03	Temperature of the heat sink surface from side opposite to the camera	35.3 ± 0.5

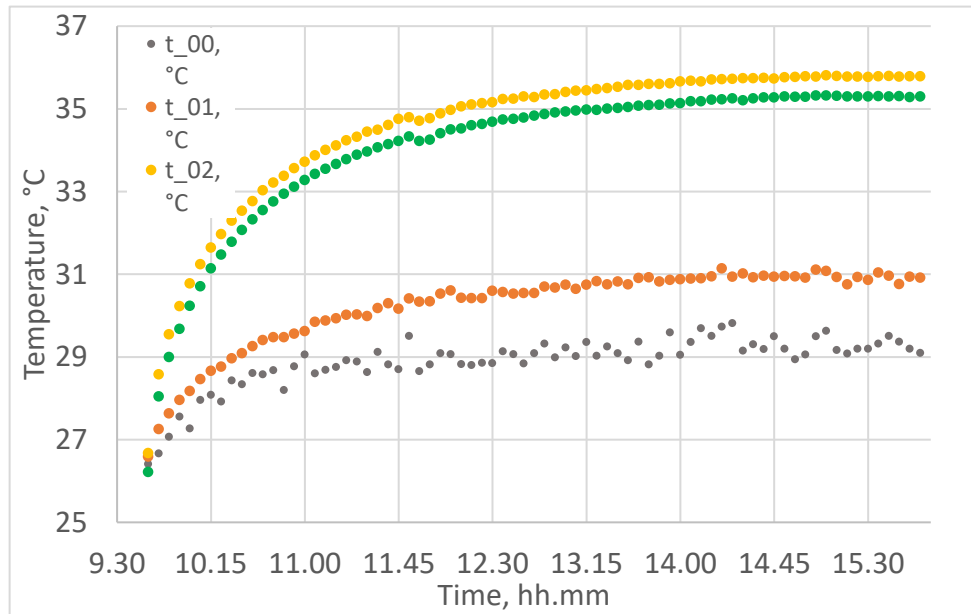


Figure 10.1. Temperature development (experiment results)

A simulation under the same operating and boundary conditions was performed to validate the model. Operating temperature was set to 30 °C. Since the LED illumination was not permanent, but intermittent, the volumetric heat source was calculated according to (18).

$$q_v = \frac{P_{nom} \cdot X}{100 \cdot V} \left[\frac{W}{m^3} \right] \quad (18)$$

where P_{nom} – nominal power of the LED strip [W]; X – percentage of LED strip illuminating in the whole scanning cycle [%], V – LED strip volume [m^3].

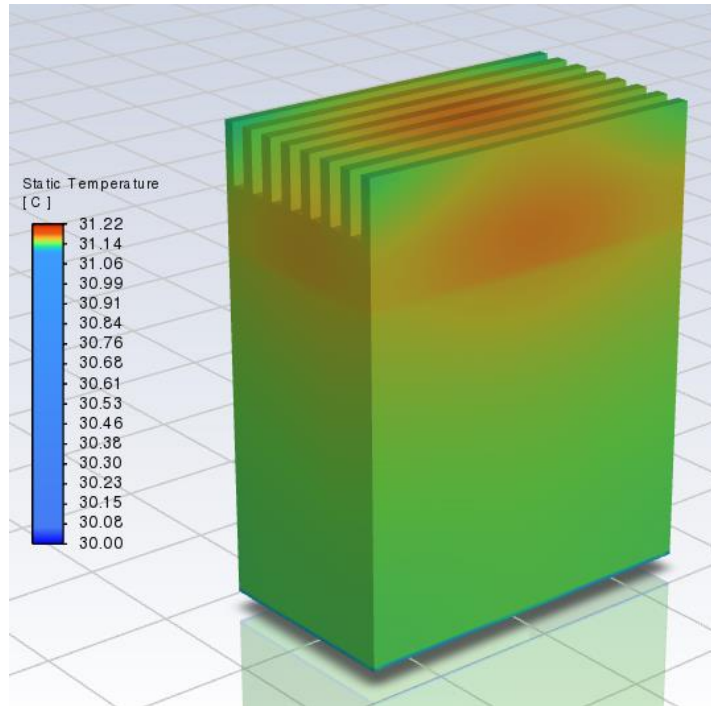


Figure 10.2. Temperature contours

The temperatures obtained from the simulation and their comparison with measured data are presented in the Table 3.

Table 3. Experimental and simulation data comparison

#		Steady temperature (experimental data), °C	Steady temperature (simulation data), °C	Difference, %
1	Air	29.3	30 (operating condition)	-
2	Air	30.9	30 (operating condition)	-
3	Cooler (camera side)	35.8	31.2	13
4	Cooler (opposite side)	35.3	31.2	12

The difference was calculated using the following formula:

$$\delta = \frac{|T_{sim} - T_{exp}|}{T_{sim}} \cdot 100 [\%] \quad (19)$$

where T_{sim} is the temperature obtained from the simulation, T_{exp} is the temperature obtained from the experiment.

The average difference between the measured temperature of the cooler and the temperature obtained from the simulation was 12.5 %. The observed difference occurs because the numerical model contained several simplifications resulting in deviations from reality.

Firstly, in order to simplify and speed up calculations the model did not include all geometric details. For instance, the absence of chamfers or grooves for wires could considerably impact the results.

Secondly, the model did not account for heat exchange by radiation which would significantly complicate the model implementation into the optimization process. However, the emissivity of the real cooler's surface treated with black anodizing is high and there is another heat source nearby – a camera located 50 mm away, reaching 60 °C during operation. Therefore, the radiation heat transfer is not negligible in the real device.

The auxiliary lights placed at the bottom of the inspection head have a further important impact which was not accounted for in the model. One of the lights is mounted straight on the main light body. This creates in principle another source of heat and heat exchange by conduction could occur between them.

Additionally, the simulation was solved as a steady-state problem, whereas in reality the LED strip's illumination process is non-uniform and cyclical. The LEDs on the strip are not continuously illuminating the product. They are active only 4 % of the entire cycle time.

Finally, the results of the calculation were influenced by the representation of ambient conditions. It would be impractical to include the entire interior of the inspection head in the model. Instead, the heat sink surroundings were represented only by the volume of air that extended by 15 mm on both sides and 55 mm above the cooler. This approximation significantly influenced the simulation results for two reasons. Firstly, the solver created fictitious air flow on the domain boundary to balance the system. Secondly, it didn't envision real air stream that was influenced by other heat sources within the device case or its' openings. Taking into account the described factors affecting the actual cooler temperature, it can be stated that the model has been successfully validated.

10.2. Optimization results

The generated data after the optimization process are shown in a figure below.

Table of Schematic G2: Optimization					
	A	B	C	D	E
1	Name	P34 - FinHeight (mm)	P35 - FinSpace (mm)	P32 - temperature-hs-op (K)	P33 - t_max_led-op (K)
2	1	14	4,7	316,12	316,82
3	2	17	4,2	315,14	315,89
4	3	12	2,2	318,21	318,82
5	4	16	3,2	315,93	316,6
6	5	11	3,7	317,57	318,2
7	6 DP 1	19	2,7		
8	7	20	5	314,12	315,31
9	8	20	5	314,12	315,31
10	9	16	4,5	315,49	316,23
11	10	19	4	314,57	315,44
12	11	18	4,7	314,67	315,53
13	12	18	3,8	315,02	315,8
14	13	20	4,8	314,14	315,26
15	14	20	5	314,12	315,31
16	15	19	4,6	314,42	315,36
17	16	18	4,9	314,72	315,62
18	17	19	4,5	314,4	315,32
19	18	19	4,8	314,38	315,35
20	19	20	5	314,12	315,31

Figure 10.3. Raw optimization data

In Figure 10.3 all simulated cases are displayed. Input parameters – the fin height and the fin spacing, are shown in the columns B and C, while the columns D and E illustrate output parameters – the average temperature of heat sink surface and the maximum temperature of the LED strip. The case 7 was not evaluated due to mesh generation failure. However, it didn't influence the optimization results since the samples with a smaller fin gap showed less effective heat dissipation.

The Figures 10.4 and 10.5 reveal iterative process of searching for optimal parameters' values. The first, second and last iterations included simulations of eight, six and five design points, respectively. The dark and the light blue lines on the graphs draw lower and upper bound values, respectively. The gap between the lines is being narrowed which indicates the solution convergence.

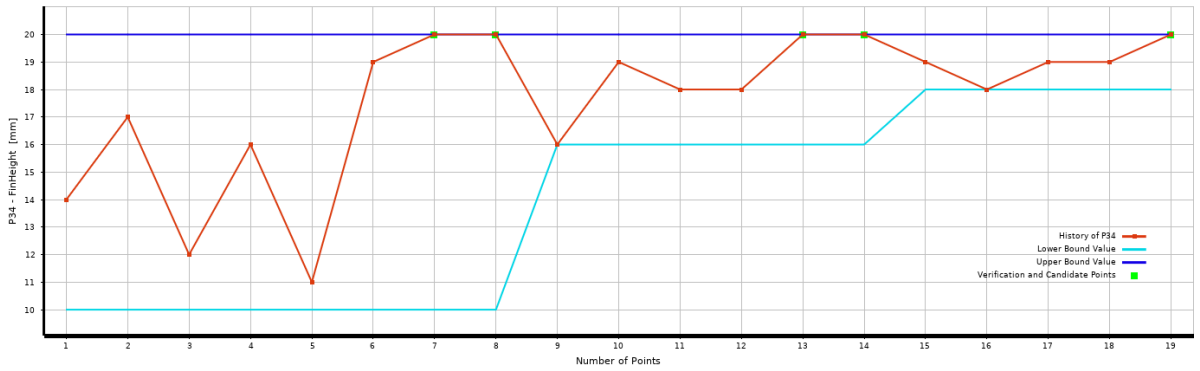


Figure 10.4. Fin height optimization development

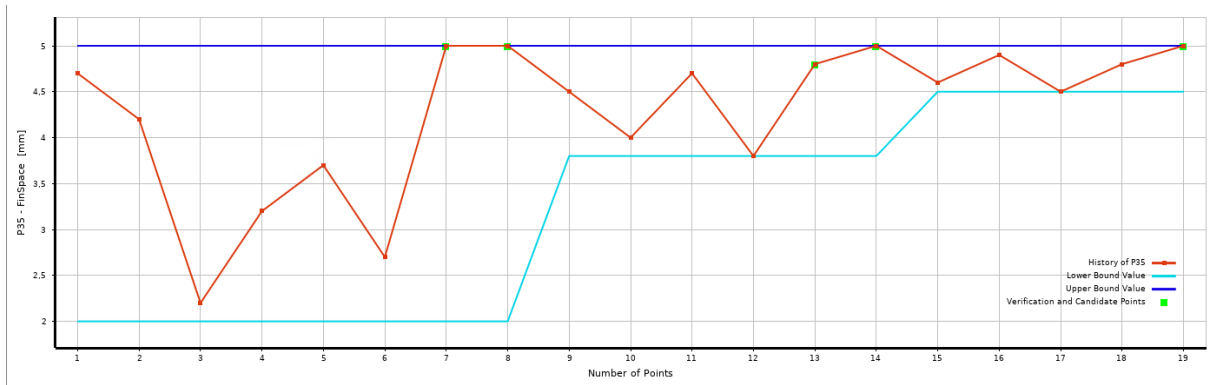


Figure 10.5. Fin spacing optimization development

The 3 candidate points are selected by the software at the end of optimization process – see Figure 10.6.

Reference	Name	P34 - FinHeight (mm)	P35 - FinSpace (mm)	P32 - temperature-hs-op (K)		P33 - t_max_led-op (K)	
				Parameter Value	Variation from Reference	Parameter Value	Variation from Reference
<input checked="" type="radio"/>	Candidate Point 1	20	5	✘✘ 314,12	0,00 %	★★★ 315,31	0,00 %
<input type="radio"/>	Candidate Point 2	19	4,8	✘✘✘ 314,38	0,08 %	★★★ 315,35	0,01 %
<input type="radio"/>	Candidate Point 3	18	4,7	✘✘✘ 314,67	0,17 %	★★★ 315,53	0,07 %

Figure 10.6. Candidate points as a result of a direct optimization

Input parameters of the Candidate Point 1 showed the biggest drop in the temperature of the cooler surface. The parameters of the optimized case and the initial case are shown in the following table.

Table 4. Optimization results

Parameter	h, mm	s, mm	T_{HS} , °C	$T_{LED MAX}$, °C
Initial case	12	3	44.3	44.9
Optimized case	20	5	41.0	42.2
Difference, %			-7.4	-6.1

The difference was calculated using the following formula:

$$\delta = \frac{|T_{init} - T_{opt}|}{T_{init}} \cdot 100 [\%] \quad (20)$$

where T_{init} is the temperature in the initial case, T_{opt} is the temperature in the optimized case.

The parametric optimization resulted in a 7.4 % reduction in the average surface temperature of the cooler, while ensuring that the temperature of the LED strip remained within the allowable limit. This improvement was achieved by increasing the fin height from 12 to 20 millimeters and the spacing between fins from 3 to 5 millimeters.

The manufacturability of the part with these parameters is a subject of discussion. With the fin spacing of 5 mm, the thickness of each fin would be only 0.875 mm. Milling such a thin fin of 20 mm height from aluminum is a highly demanding goal due to possible metal deformation and tool limitations. However, an alternative manufacturing approach can be considered: grooves with a width of 1 mm could be milled in the base, into which thin plates, cut from a 1 mm thick aluminum sheet, would be inserted and soldered. This method would guarantee that the geometry of the part closely aligns with the optimal design while remaining manufacturable. An alternative manufacturing method for such a part is extrusion. In extrusion, an aluminum alloy is pushed through a die with specific geometric parameters (profile). Using this method, it would be possible to produce even thinner fins.

11. Conclusion

The objective of the master thesis was to perform parametric optimization of a light source cooler. A literature review on heat sinks and methods to improve their efficiency was conducted. The literature analysis revealed that the cooling performance of a heat sink is influenced by several factors, including material, dimensions, shape and topology, ambient environment (air or liquid), cooling mode (active or passive) and others.

Ansys software was used for the optimization. The geometry modeling, meshing, and thermal analysis with natural convection simulation were conducted using Ansys Design Modeler, Ansys Meshing and Ansys Fluent, respectively. An experiment to measure the surface temperature of the cooler was carried out to validate the model. The temperatures obtained from the simulation and the measured temperatures differed by an average of 12.5 %. This discrepancy can be attributed to several simplifications in the model, such as the exclusion of radiation effects, absence of geometric features (chamfers and holes), and the limited computational domain size (volume of air surrounding the heat sink). Simulating a model that fully reflects reality would require immense computational resources, which is at present neither feasible nor rational. Considering this, it can be asserted that the computational model was successfully validated.

The Ansys Direct Optimization and Parameter Set modules in Ansys Workbench were studied for the optimization process. The fin height and the distance between fins were chosen as optimized parameters, with the objective of reducing the average temperature of the cooler. Additionally, a constraint was assigned, limiting the maximum LED strip temperature to 100 °C. The Adaptive Single-Objective method was selected for the optimization. Given that there were only two input parameters and one objective, the solution converged in just three iterations.

The optimization process resulted in 7.6% reduction of the average heat sink surface temperature, with the LED strip temperature still below the maximum allowed value. Achieving this required increasing the fin height to 20 mm and the fin spacing to 5 mm. It is noteworthy that these numbers were the upper limits of acceptable values for these parameters, considering the maximum permissible cooler dimensions and the manufacturing possibilities. The initial heat sink was produced on a milling machine with its dimensions constrained by milling capabilities. The optimized heat sink cannot be

manufactured using the same method due to the fin dimensions (with 5 mm spacing, each fin would be 0.875 mm thick). Therefore, alternative manufacturing methods such as soldering thin plates to the base or extrusion were proposed.

The thesis objective was achieved, but the topic still has a potential for further exploration. For instance, the optimization could extend beyond fin height and width to include fin count and shape. Additionally, fins could be non-uniform (varying height and width, denser fin placement in certain areas, etc.). Another way of improvement would be adding perpendicular grooves to the fins on the existing geometry to influence airflow around the cooler, potentially enhancing its cooling performance.

References

- [1] LIU, Ping; SUN, Ruiqi; HU, Lianghong; WANG, Weihua a JI, Jiadong. Heat Transfer Enhancement of Microchannel Heat Sink Using Sine Curve Fins. *Journal of Thermophysics and Heat Transfer*. ISSN 0887-8722. Available from: <https://doi.org/10.2514/1.T6967>.
- [2] TONG H.-M., LAI Y.-S., WONG C. *Advanced flip chip packaging*. Boston, MA: Springer US, 2013. ISBN 978-1-4419-5767-2. Available from: <https://doi.org/10.1007/978-1-4419-5768-9>.
- [3] HU, Yuanchen; SARVEY, Thomas; BAKIR, Muhannad S. a JOSHI, Yogendra. Single Phase Liquid Cooling of High Heat Flux Devices With Local Hotspot in a Microgap With Nonuniform Fin Array. *Journal of Heat Transfer*. 2021, 143(3). ISSN 0022-1481. Available from: <https://doi.org/10.1115/1.4049189>.
- [4] LUO, Xiaobing; HU, Run; LIU, Sheng a WANG, Kai. Heat and fluid flow in high-power LED packaging and applications. *Progress in Energy and Combustion Science*. 2016, 56, pp. 1-32. ISSN 03601285. Available from: <https://doi.org/10.1016/j.pecs.2016.05.003>.
- [5] HUI, S. Y. R., QIN, Y. X. A General Photo-Electro-Thermal Theory for Light Emitting Diode (LED) Systems. *Twenty-Fourth Annual IEEE Applied Power Electronics Conference and Exposition*, Washington, DC, USA, 2009, pp. 554-562, doi: 10.1109/APEC.2009.4802712.
- [6] CHENG, J. H., LIU, C. K., CHAO, Y. L., TAIN, R. M. Cooling performance of silicon-based thermoelectric device on high power LED. *In Proc. 24th Int. Conf. Thermoelectrics*, Clemson, SC, Jun. 2005, pp. 53–56.
- [7] ZAHNER, T. Thermal management and thermal resistance of high power LEDs. *In Proc. 13th Int. Workshop Thermal Investigation ICs Syst. THERMINIC 2007*, Budapest, Hungary, Sep., pp. 195–195.
- [8] MURSHED, S.M. Sohel. *Electronics Cooling*. Zagreb: InTech, 2016. ISBN 978-953-51-2405-4. Available from: <https://doi.org/10.5772/63321>.
- [9] AHMADIANFAR, Iman; BOZORG-HADDAD, Omid, CHU, Xuefeng. Gradient-based optimizer: A new metaheuristic optimization algorithm. *Information Sciences*. 2020, 540, pp. 131-159. ISSN 00200255. Available from: <https://doi.org/10.1016/j.ins.2020.06.037>.
- [10] ROTHLAUF, Franz. *Design of Modern Heuristics. Natural Computing Series*. Berlin, Heidelberg: Springer, 2011. ISBN 978-3-540-72961-7. Available from: <https://doi.org/10.1007/978-3-540-72962-4>.
- [11] SAGIMBAYEV, Sagi; KYLYSHBEK, Yestay; BATAY, Sagidolla; ZHAO, Yong; FOK, Sai et al. 3D Multidisciplinary Automated Design Optimization Toolbox for Wind Turbine Blades. *Processes*. 2021, 9(4). ISSN 2227-9717. Available from: <https://doi.org/10.3390/pr9040581>.
- [12] COSTA, Vítor A.F., LOPES, António M.G. Improved radial heat sink for led lamp cooling. *Applied Thermal Engineering*. 2014, 70(1). ISSN 13594311. Available from: <https://doi.org/10.1016/j.applthermaleng.2014.04.068>.

- [13] CULHAM, J. R., MUZYCHKA, Y. S. Optimization of plate fin heat sinks using entropy generation minimization. *IEEE Transactions on Components and Packaging Technologies*, vol. 24, no. 2, June 2001, doi: 10.1109/6144.926378.
- [14] DEDE, E. M., JOSHI, S. N., ZHOU, F. (October 12, 2015). Topology Optimization, Additive Layer Manufacturing, and Experimental Testing of an Air-Cooled Heat Sink. *ASME Journal of Mechanical Design*. November 2015; 137(11): 111403. <https://doi.org/10.1115/1.4030989>.
- [15] PILAGATTI, Adriano Nicola; PISCOPO, Gabriele; ATZENI, Eleonora; IULIANO, Luca, SALMI, Alessandro. Design of additive manufactured passive heat sinks for electronics. *Journal of Manufacturing Processes*. 2021, 64. ISSN 15266125. Available from: <https://doi.org/10.1016/j.jmapro.2021.01.035>.
- [16] GHAZI, T., ATTAR, M. R., GHORBANI, A., ALSHIHMANI, H., DAVOODI, A., PASSANDIDEH-FARD, M., SARDARABADI, M. (2023). Synergistic effect of active-passive methods using fins surface roughness and fluid flow for improving cooling performance of heat sink heat pipes. *Experimental Heat Transfer*, 1–16. <https://doi.org/10.1080/08916152.2023.2182838>.
- [17] HABIB, Numan; SIDDIQI, Muftooh a TAHIR, Muhammad. Thermal analysis of proposed heat sink design under natural convection for the thermal management of electronics. *Thermal Science*. 2022, 26(2) Part B, pp. 1487-1501. ISSN 0354-9836. Available from: <https://doi.org/10.2298/TSCI210402307H>.
- [18] BARTÁK, M. *Úvod do přenosových jevů pro inteligentní budovy*. Elektronická příručka (PDF). 2010.
- [19] YUNUS A. C., AFSHIN J. G. *Heat and Mass Transfer: Fundamentals and Applications*. 5th ed. New York, NY: McGraw-Hill Professional (2014).
- [20] BAR-COHEN A., ROHSENOW W. M. Thermally Optimum Spacing of Vertical Natural Convection Cooled Parallel Plates. *Journal of Heat Transfer* 106 (1984).
- [21] KURTARAN, H., ERZURUMLU, T. (2005). Efficient warpage optimization of thin shell plastic parts using response surface methodology and genetic algorithm. *The International Journal of Advanced Manufacturing Technology*, 27(5-6), 468-472. doi:10.1007/s00170-004-2321-2.
- [22] ANSYS Workbench, 2023 R2. ANSYS, Inc.
- [23] ANSYS Fluent, 2023 R2, *ANSYS Fluent Theory Guide*, ANSYS, Inc.
- [24] MENTER F.R., LECHNER R., MATYUSHENKO A., NTS. *Best Practice: RANS Turbulence Modeling in Ansys CFD* (2021). ANSYS, Inc.
- [25] TYFLOPOULOS, Evangelos, STEINERT, Martin. Topology and Parametric Optimization-Based Design Processes for Lightweight Structures. *Applied Sciences*. 2020, 10(13): ISSN 2076-3417. Available from: <https://doi.org/10.3390/app10134496>.

Appendix I. Thermal paste datasheet



PRODUCT DATA SHEET Thermal Grizzly Hydronaut

Description:
Thermal Grizzly Hydronaut is a high performance thermal grease.

Properties:
Thermal Grizzly Hydronaut is a very high performance thermal grease, which shows its true capabilities in cryogenic environments. Hydronaut thermal grease sports high long time stability, all without curing. Hydronaut thermal grease is silicone-free.

Applications:
Thermal Grizzly Hydronaut is best used with applications in need of high temperature resistance, for example those in electrical or computer engineer-

ring. Of course, Thermal Grizzly Hydronaut can also be used in a wide variety of other lines of industries. Hydronaut thermal grease was created especially for larger-scale cooling solutions. Thermal Grizzly Hydronaut is best applied with the Thermal Grizzly applicator, but it can also be applied by way of brush, spatula, silkscreen or pad printing.

Storage:
Thermal Grizzly Hydronaut should be stored in its original packaging, in a dry environment at room temperature.



Property	Value/Description	Property	Value/Description
Viscosity	140–190 Pas	Standard Sizes	3ml, 1,5ml, 1g
Density	2.6g/cm ³	Possible Thickness	variable
Application Temperature	-200° C to 350° C	Silicone based	no
Electrical Conductivity*	0 pS/m	Typical Application	CPUs, GPUs, Notebooks, ICs
Consistency	soft		
Colour	light grey		

*following DIN 51412-1
All of these data were determined and confirmed with the technical facilities of <http://overclocking.guide>.

Trademark Information:
Thermal Grizzly is a registered trademark.

Please note:
The data in this technical data sheet are based on our current knowledge and experience. Due to the large amount of possible factors, this should not be construed as to release the users from doing their own

tests and screening. No legally binding assurance of specific properties or applicability for a concrete purpose should be derived from these data. Please consider contacting us for further detail.

It is the responsibility of the recipient of our products to ensure that any proprietary rights and existing laws and legislation are observed.

TGU20212309

Thermal Grizzly – High Performance Cooling Solutions
 Egelpfuhlstrasse 44 · 13581 Berlin · Germany
 Phone +49-40-53 27 88 50 · Fax +49-321-21 13 47 93
 sales@thermal-grizzly.com
 CEO: Eike Salow · USt-IdNr. DE270324124

Appendix II. PT100 thermometer tolerances



PT100 Tolerance Information

**PT100 Resistance Thermometer Tolerance Chart
Relating to EN 60751 1996 and 2008**

PT100 Temperature Tolerance (+/- °C)				
Temperature °C	EN 60751 1996 Class B	EN 60751 1996 Class A	1/3 DIN	1/10 DIN (not in standard)
	EN 60751 2008 Class B	EN 60751 2008 Class A	EN 60751 2008 Class AA	
-196	1.28			
-100	0.80	0.35		
-80	0.70	0.31		
-50	0.55	0.25	0.19	
-25	0.43	0.20	0.14	
0	0.30	0.15	0.10	0.03
25	0.43	0.20	0.14	0.04
50	0.55	0.25	0.19	0.06
75	0.68	0.30	0.23	0.07
100	0.80	0.35	0.27	0.08
125	0.93	0.40	0.31	
150	1.05	0.45	0.36	
175	1.18	0.50	0.40	
200	1.30	0.55	0.44	
225	1.43	0.60	0.48	
250	1.55	0.65	0.53	
275	1.68	0.70		
300	1.80	0.75		
325	1.93	0.80		
350	2.05	0.85		
375	2.18	0.90		
400	2.30	0.95		
425	2.43	1.00		
450	2.55	1.05		
475	2.68			
500	2.80			
550	3.05			
600	3.30			



Wire Wound Detector
Thin Film Detector

In accordance with BS EN 60751 : 1996 and 2008
Resistance at 0.0°C = 100 ohms
Alpha value = 0.00385 Ω/Ω/°C

Thermal Detection Limited
Unit 6, Primrose Hill Industrial Estate
Orde Wingate Way
Stockton-on-Tees, England,
TS19 0GA

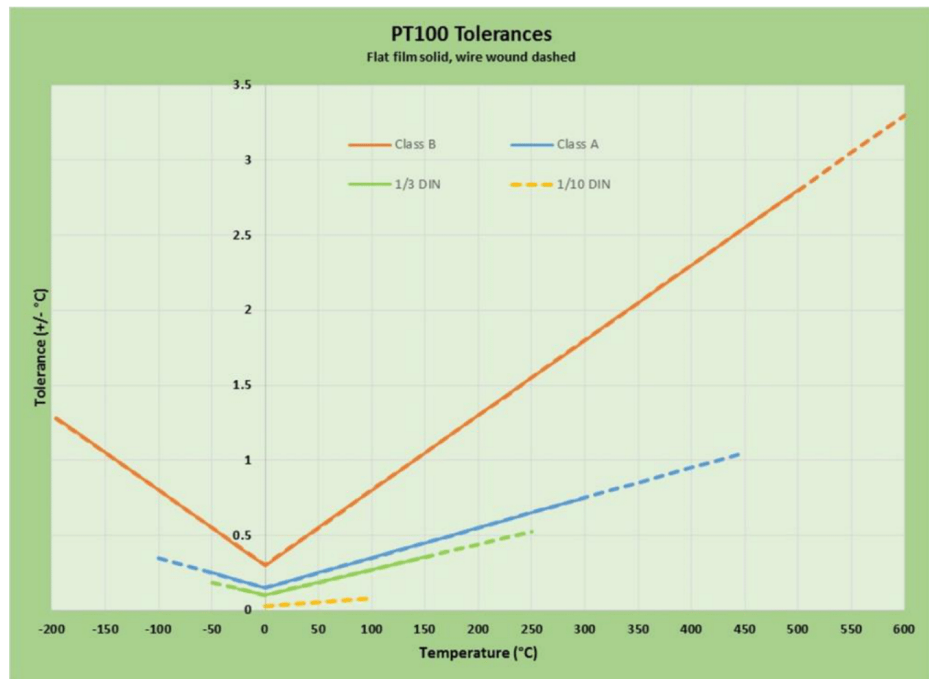


Fax : +44 (0) 1642 618307
Tel : +44 (0) 1642 602878
Email: sales@thermal-detection.com
Web: www.thermal-detection.com
© Thermal Detection Ltd 2016



PT100 Tolerance Information

PT100 Resistance Thermometer Tolerance Chart



Thermal Detection Limited
Unit 6, Primrose Hill Industrial Estate
Orde Wingate Way
Stockton-on-Tees, England,
TS19 0GA



Fax : +44 (0) 1642 618307
Tel : +44 (0) 1642 602878
Email: sales@thermal-detection.com
Web: www.thermal-detection.com
© Thermal Detection Ltd 2016

Appendix III. Ansys Direct Optimization setup

The Direct Optimization tool can be found in Ansys Workbench on the *Toolbox* menu in the *Design Exploration* section.

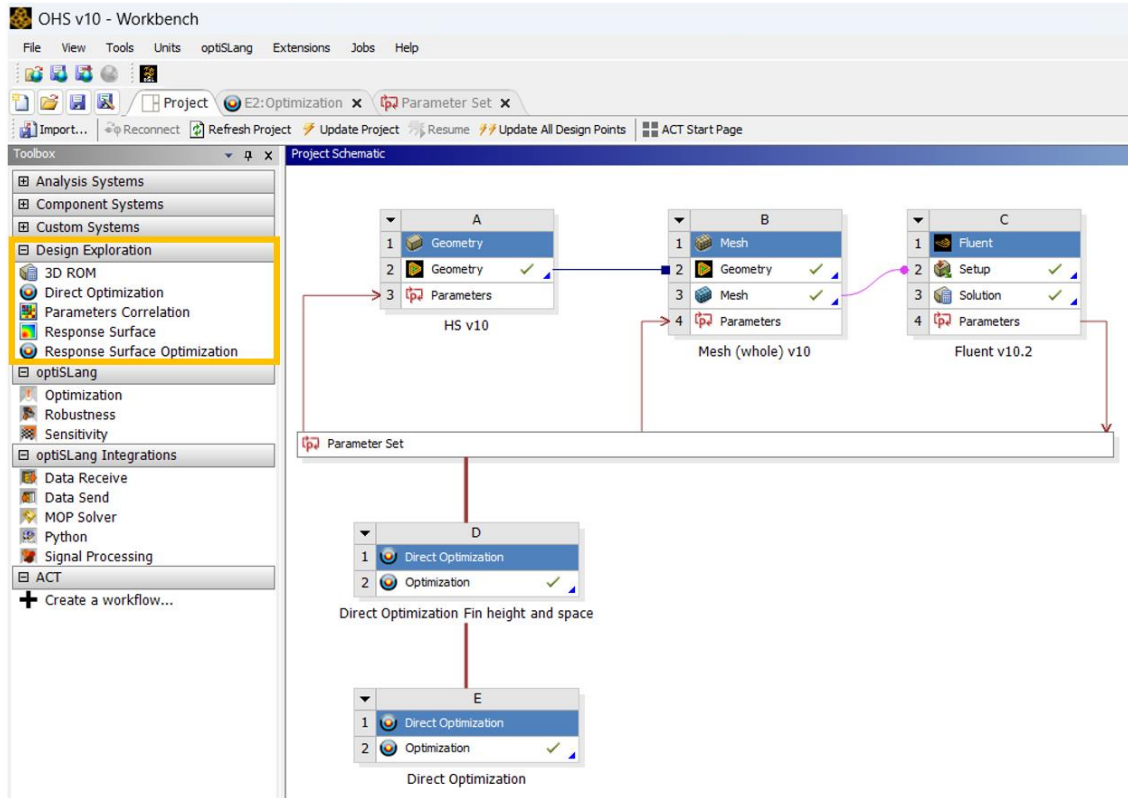


Figure III.1. Workbench Toolbox options and Project Schematic

Direct Optimization belongs to parametric optimization approaches. Thus, the optimization parameters should be specified.

Input parameters are entered by a user and these are the optimized ones. Any numerical value entered by a user can be selected as an input parameter. In such tools as Design Modeler or Meshing, a parameter can be set by clicking on a white checkbox on the left of the input value. In Ansys Fluent, a quantity is designated as a parameter from a drop-down list on the right of the input value. After a quantity is selected as an input parameter, its value can be changed manually from the Parametric Set only.

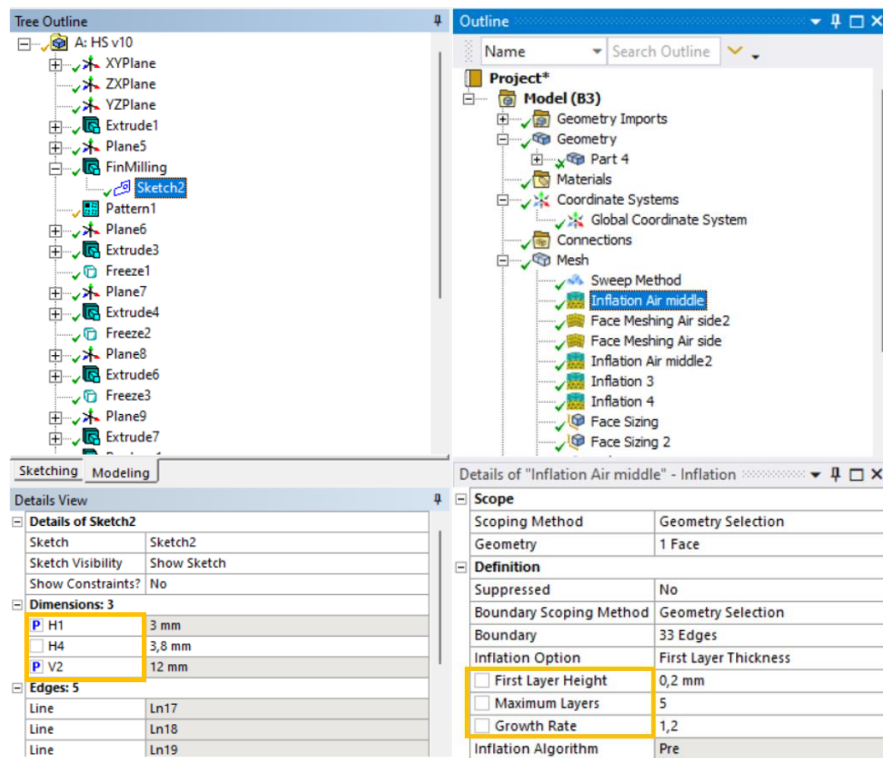


Figure III.2. Input parameters in Design Modeler (on the left) and Meshing (on the right). “P” in a checkbox indicates, that a value is selected as an input parameter. The gray background in a value field denotes that it cannot be edited manually from this menu.

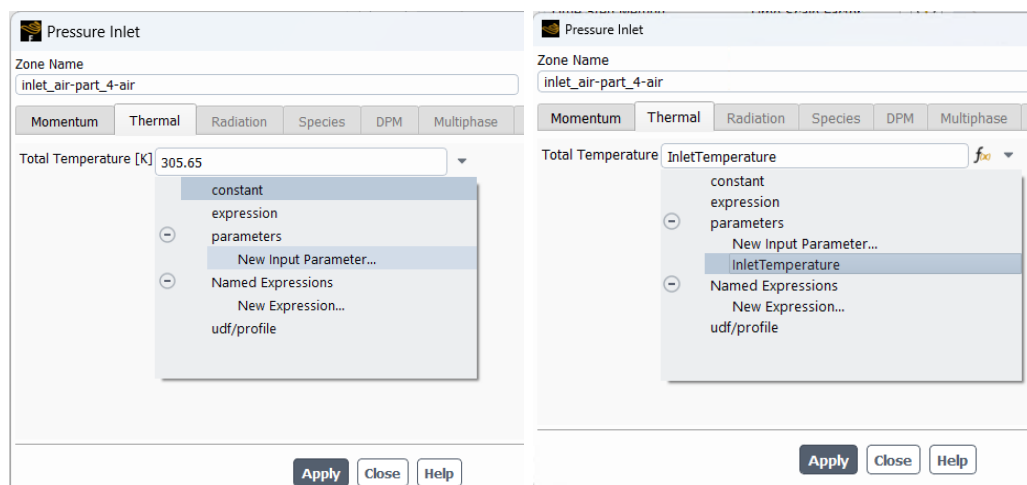


Figure III.3. Setting an input parameter in Fluent

Output parameters are obtained as a result of the mesh generation or the simulation. They are used in an optimization process for objective and constraint definitions. In Meshing, a parameter can be set by clicking on a white checkbox on the left of the output value. In Ansys Fluent, output parameters are created from report definitions by clicking on a “Create Output Parameter” button. In Fluent, all input and output parameters are shown on the *Outline View* pane in the *Parameters & Customization* section.

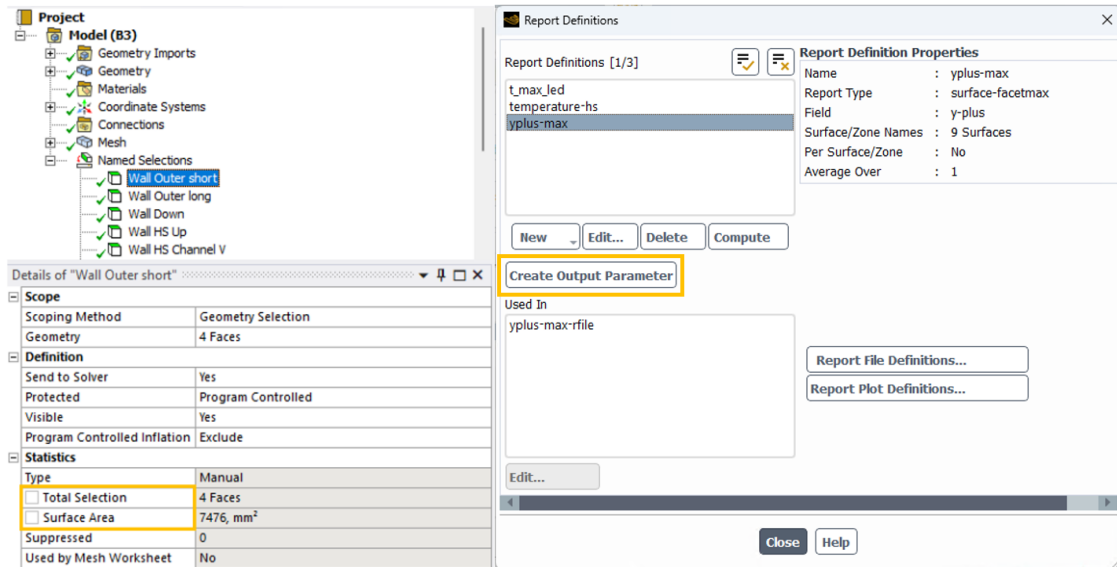


Figure III.4. Creating output parameters in Meshing (on the left) and Fluent (on the right)

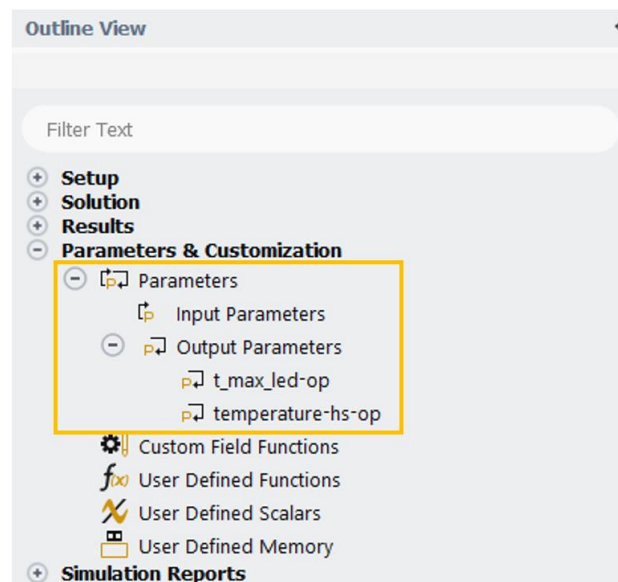


Figure III.5. Overview of parameters in Fluent

After input/output parameters are selected, a Parameter Set box is automatically added to the Project Schematic. Arrows are connecting Parameter Set to individual blocks representing parameter definition. An arrow pointing towards a block indicates an input parameter, while an arrow pointing away from a block indicates an output parameter.

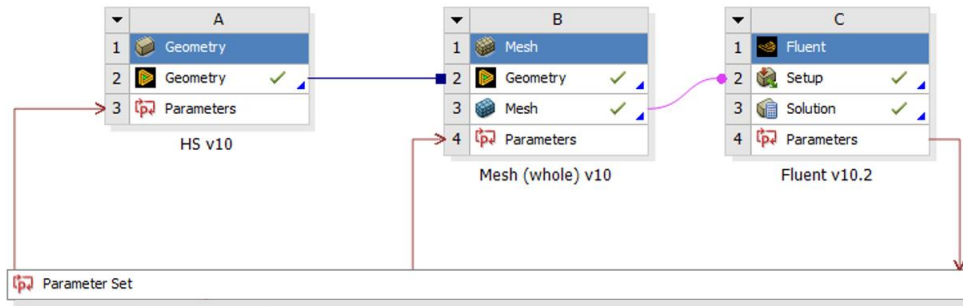


Figure III.6. Project Schematic after defining parameters

Outline of All Parameters				
	A	B	C	D
1	ID	Parameter Name	Value	Unit
2	Input Parameters			
3	HS v10 (A1)			
4	P34	FinHeight	12	mm
5	P35	FinSpace	3	mm
*	New input parameter	New name	New expression	
7	Output Parameters			
8	Fluent v10.2 (D1)			
9	P32	temperature-hs-op	317,41	K
10	P33	t_max_jed-op	318,03	K
*	New output parameter		New expression	
12	Charts			

Figure III.7. Parameter Set

The Direct Optimization tool is then linked to the Parameter Set. Several optimization blocks can be connected to one Parameter Set. Optimization processes in this case are solved independently.

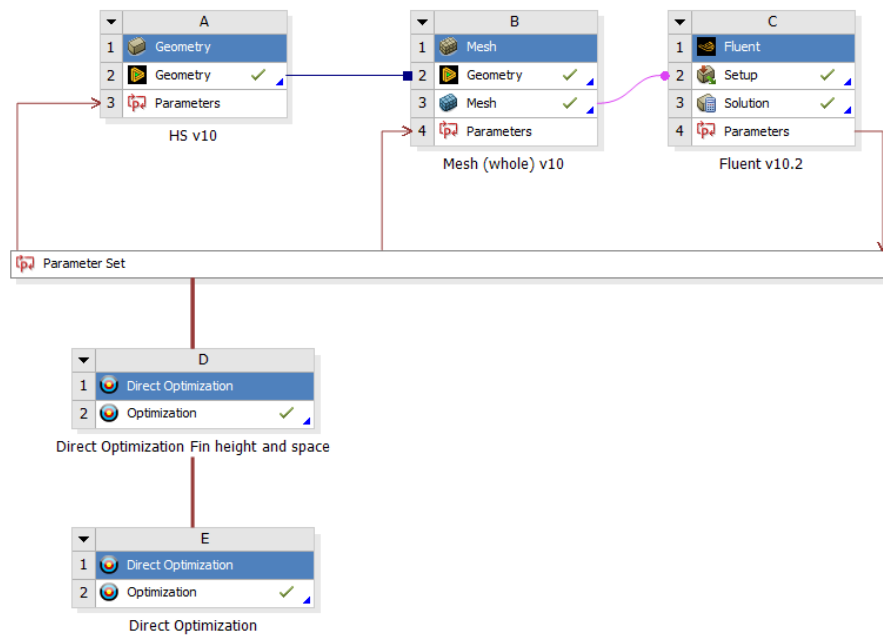


Figure III.8. Project Schematic with Optimization tools

If no parameters are defined prior to inserting Direct Optimization to the Project Schematic, an empty Parameter Set is created automatically. Parameters can be defined later and will be connected to the Parametric Set.

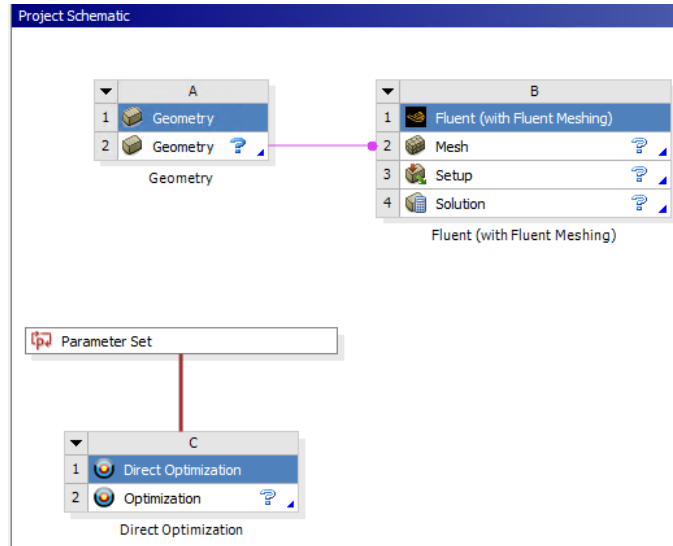


Figure III.9. Example of a Direct Optimization block inserted to a project with no predefined parameters

The Direct Optimization module is not a separate software, but a tool that can be used within Ansys Workbench platform. Its setup and results are shown in a separate tab in the Workbench window. An optimization setup involves choosing objectives and constraints, defining optimized parameters' range and allowed values, selecting optimization method and properties.

Input parameters are automatically inserted into the optimization tree from a Parametric Set. If a parameter is not included into this optimization process, it can be disabled in a checkbox on the right of a parameter name.

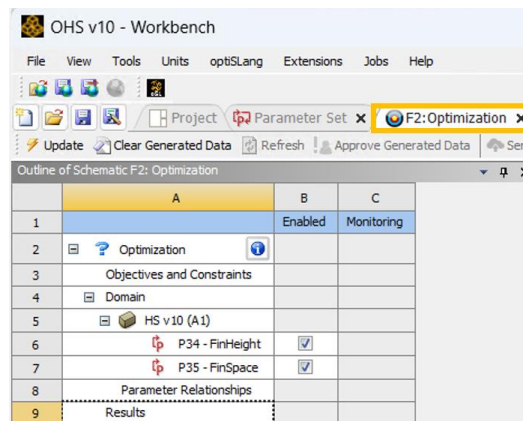


Figure III.10. Direct Optimization tab in Ansys Workbench

Lower and upper bounds for each parameter should be set. Allowed values interval can be floating (*Any*), fixed (*Snap to Grid*) or predefined by a user (*Manufacturable Values*). It is necessary to specify starting values for NLPQL and MISQP optimization methods (see Chapter 7).

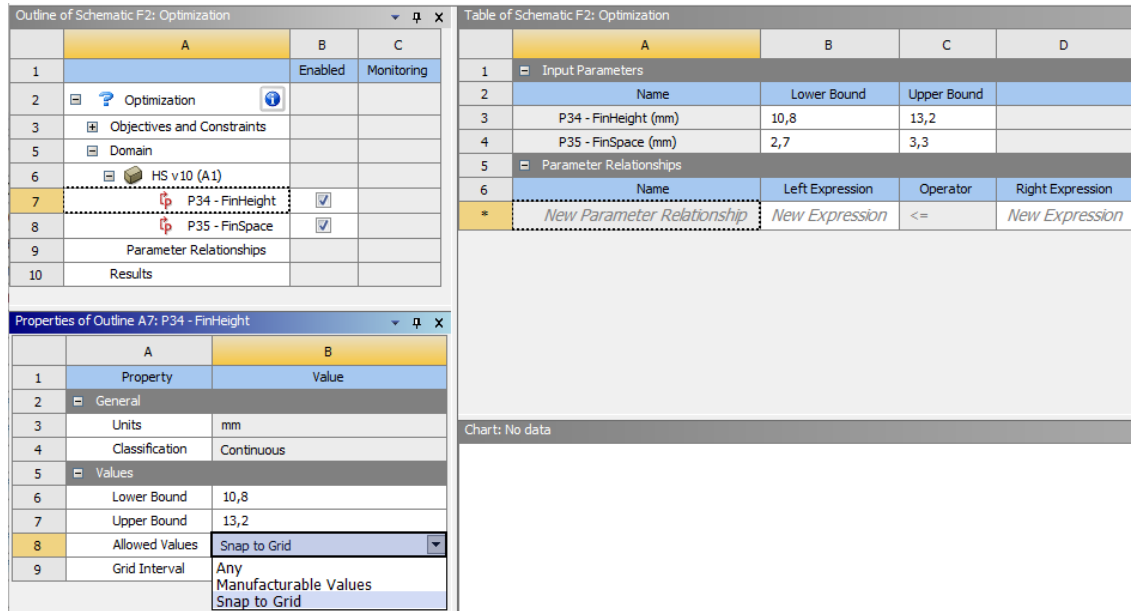


Figure III.11. Optimized parameters setup

Any parameter (input or output) can have an objective and/or constraint. In this step an optimization goal and conditions are set. A parameter can be either **minimized**, **maximized** or optimized to closely **approximate a specific value**. Constraints define allowed range for the values. Objectives and constraints are described in the same section and are presented in one table (see Figure III.14).

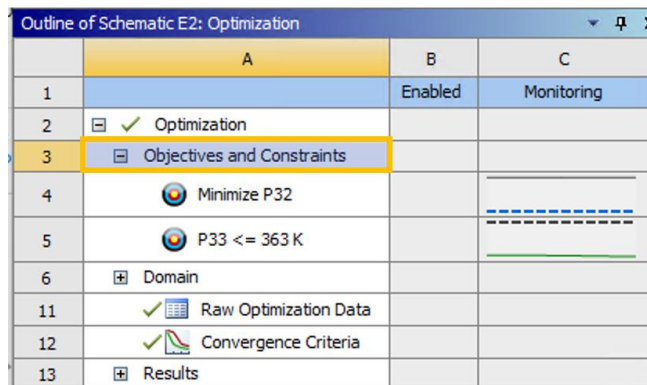


Figure III.12. Objectives and constraints section

Table of Schematic F2: Optimization									
	A	B	C	D	E	F	G	H	I
1	Name	Parameter	Objective			Constraint			
2			Type	Target	Tolerance	Type	Lower Bound	Upper Bound	Tolerance
3	P32	P32 - temperature-hs-op	No Objective			No Constraint			
*		Select a Parameter	No Objective Minimize Maximize Seek Target						

Figure III.13. Objective options

Table of Schematic F2: Optimization									
	A	B	C	D	E	F	G	H	I
1	Name	Parameter	Objective			Constraint			
2			Type	Target	Tolerance	Type	Lower Bound	Upper Bound	Tolerance
3	P32	P32 - temperature-hs-op	No Objective			No Constraint			
*		Select a Parameter	No Constraint Values <= Upper Bound Values >= Lower Bound Values = Bound Lower Bound <= Values <= Upper						

Figure III.14. Constraint options

Table of Schematic E2: Optimization									
	A	B	C	D	E	F	G	H	I
1	Name	Parameter	Objective			Constraint			
2			Type	Target	Tolerance	Type	Lower Bound	Upper Bound	Tolerance
3	Minimize P32	P32 - temperature-hs-op	Minimize	0		No Constraint			
4	P33 <= 363 K	P33 - t_max_led-op	No Objective			Values <= Upper Bound		363	0,001
*		Select a Parameter							

Figure III.15. Objectives and constraints setup

Optimization setup includes a method selection and optionally optimization properties definition. If the automatic selection is chosen, most of the properties are regulated by a single value – the *Run Time Index*. A higher value of the *Run Time Index* would extend the optimization process but may result in a more accurate output.

Outline of Schematic E2: Optimization			
	A	B	C
1		Enabled	Monitoring
2	✓ Optimization		
3	⊕ Objectives and Constraints		
6	⊕ Domain		
11	✓ Raw Optimization Data		
12	✓ Convergence Criteria		
13	⊕ Results		

Figure III.16. Optimization section

Properties of Outline A2: Optimization		
	A	B
1	Property	Value
2	+ Design Points	
4	+ Failed Design Points Management	
6	- Optimization	
7	Method Selection	Auto
8	Run Time Index	5 - Medium
9	Estimated Number of Design Points	1 - Quick 2 3 4
10	Method Name	5 - Medium
11	Tolerance Settings	6 7
12	Number of Initial Samples	8 9 - Long

Figure III.17. Run Time Index

A wide range of optimization methods can be selected manually. The methods are listed and described in the Chapter 7. Properties differ with respect to individual methods. Some examples can be seen on the next figures.

Properties of Outline A2: Optimization		
	A	B
1	Property	Value
2	+ Design Points	
4	+ Failed Design Points Management	
6	- Optimization	
7	Method Selection	Manual
8	Method Name	MOGA
9	Estimated Number of Design Points	1050
10	Tolerance Settings	<input checked="" type="checkbox"/>
11	Number of Initial Samples	100
12	Number of Samples Per Iteration	50
13	Maximum Allowable Pareto Percentage	70
14	Convergence Stability Percentage	2
15	Maximum Number of Iterations	20
16	Maximum Number of Candidates	3
17	+ Optimization Status	
24	+ Design Point Report	

Properties of Outline A2: Optimization		
	A	B
1	Property	Value
2	+ Design Points	
4	+ Failed Design Points Management	
6	- Optimization	
7	Method Selection	Manual
8	Method Name	NLPQL
9	Estimated Number of Design Points	60
10	Tolerance Settings	<input checked="" type="checkbox"/>
11	Finite Difference Approximation	Forward
12	Allowable Convergence (%)	0,1
13	Maximum Number of Iterations	20
14	Maximum Number of Candidates	3
15	+ Optimization Status	
22	+ Design Point Report	

Figure III.18. Optimization properties of MOGA and NLPQL methods

After the optimization setup is done, the process can be started by clicking the *Update* button. The optimization procedure is described more detailed in Chapter 7. After the process is finished a table of Raw Optimization Data is generated. It contains

all estimated samples (design points, DPs). It is possible that output parameters at some design points will not be estimated due to unphysical geometry, mesh failures or other errors. In this case a lightning icon with a red cross appear at the relevant raw.

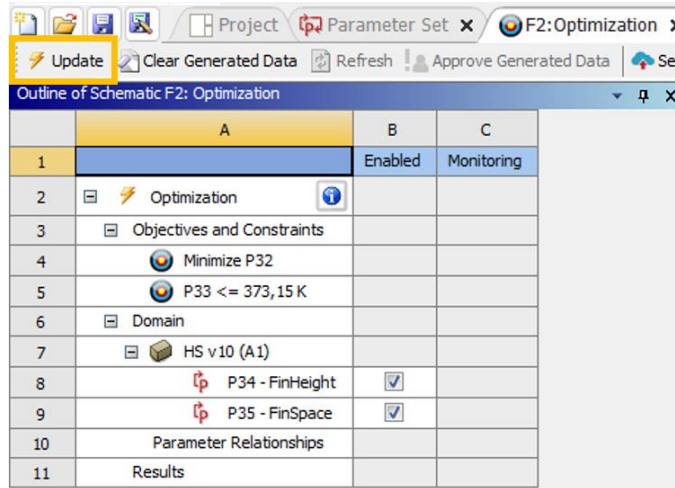


Figure III.19. Optimization process start

Table of Schematic F2: Optimization					
	A	B	C	D	E
1	Name	P34 - FinHeight (mm)	P35 - FinSpace (mm)	P32 - temperature-hs-op (K)	P33 - t_max_led-op (K)
2	1	14	4,7	316,12	316,82
3	2	17	4,2	315,14	315,89
4	3	12	2,2	318,21	318,82
5	4	16	3,2	315,93	316,6
6	5	11	3,7	317,57	318,2
7	6 DP 1	19	2,7	⚡	⚡
8	7	20	5	314,12	315,31
9	8	20	5	314,12	315,31
10	9	16	4,5	315,49	316,23
11	10	19	4	314,57	315,44
12	11	18	4,7	314,67	315,53
13	12	18	3,8	315,02	315,8
14	13	20	4,8	314,14	315,26
15	14	20	5	314,12	315,31
16	15	19	4,6	314,42	315,36
17	16	18	4,9	314,72	315,62
18	17	19	4,5	314,4	315,32
19	18	19	4,8	314,38	315,35
20	19	20	5	314,12	315,31

Figure III.20. Raw optimization data

Post-process analytics is also realized in the Direct Optimization tool in the *Results* section. *Candidate points* that best fit the criteria are automatically selected and estimated. For gradient-based single-objective methods one candidate point is enough and will be the optimal solution of a problem. Other methods might need more candidate points to be estimated. The variation of output parameters is also calculated with regard to the reference point. The reference design point can be either an initial case or another sample chosen by a user.

Outline of Schematic E2: Optimization			
	A	B	C
1		Enabled	Monitoring
2	Optimization		
3	Objectives and Constraints		
6	Domain		
11	Raw Optimization Data		
12	Convergence Criteria		
13	Results		
14	Candidate Points		
15	Tradeoff		
16	Samples		

Figure III.21. Results section

Table of Schematic F2: Optimization , Candidate Points								
	A	B	C	D	E	F	G	H
1	Reference	Name	P34 - FinHeight (mm)	P35 - FinSpace (mm)	P32 - temperature-hs-op (K)		P33 - t_max_led-op (K)	
2					Parameter Value	Variation from Reference	Parameter Value	Variation from Reference
3	●	Candidate Point 1	20	5	314,12	0,00 %	315,31	0,00 %
4	○	Candidate Point 2	19	4,8	314,38	0,08 %	315,35	0,01 %
5	○	Candidate Point 3	18	4,7	314,67	0,17 %	315,53	0,07 %
*		New Custom Candidate Point	15	3,5				

Figure III.22. Candidate points chosen by the optimization tool

The *Convergence Criteria* chart is generated and can be monitored during the optimization process. Its content varies for single- and multiple-objective methods. An example of the *Convergence Criteria* chart is presented on the Figure III.23. Another way to visualize and interpret the results is to demonstrate the design points on the *Samples Chart*. Each case is represented on the chart by one color and connects its input and output parameters values. Values, number of samples and the way of their representation can be defined in the settings panel.

Properties of Outline : Samples			
	A	B	C
1	Property	Value	Enab..
2	Chart		
3	Display Parameter Full Name	<input type="checkbox"/>	
4	Mode	Pareto Fronts	
5	Number of Pareto Fronts to Show	3	
6	Coloring method	by Pareto Front	
7	Show Infeasible Points	<input type="checkbox"/>	
8	Input Parameters		
9	P34 - FinHeight	20	<input checked="" type="checkbox"/>
10	P35 - FinSpace	5	<input checked="" type="checkbox"/>
11	Output Parameters		
12	P32 - temperature-hs-op	314,12	<input checked="" type="checkbox"/>
13	P33 - t_max_led-op	315,31	<input checked="" type="checkbox"/>

Figure III.23. Samples Chart settings panel

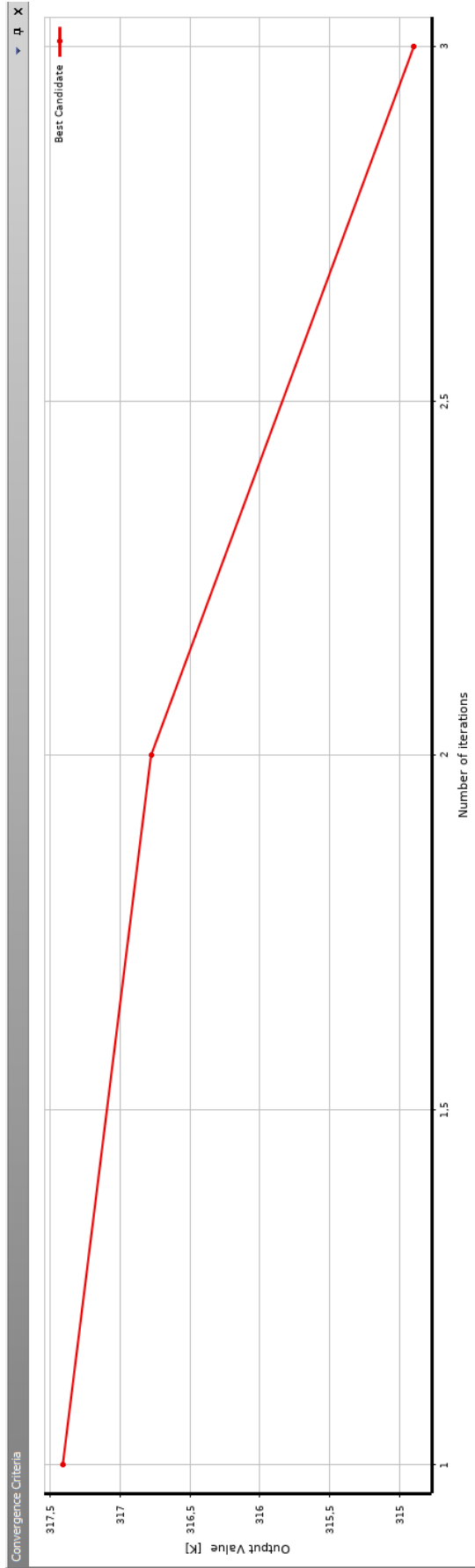


Figure III.24. Convergence Criteria chart of a single-objective optimization method. The evolution of the best candidate point in each iteration

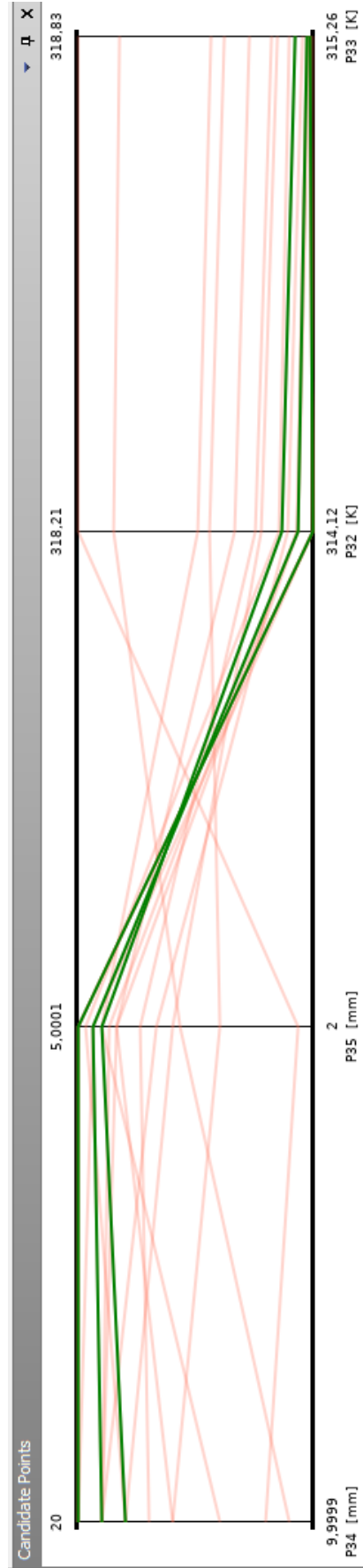


Figure III.25. Samples Chart